4 CFD Modelling of Boiler

4.1 Two-Phase Flow and Flow in Tube Banks

4.1.1 Introduction

Due to the fact that most of the erosion occurs in and around boiler tube banks is it important to know how two-phase flow behaves around these tubes. A fair amount of research has been done on erosion of single tubes as well as of multiple tubes. The multiple tubes are configured either in a staggered or an in-line arrangement. Table 4-1 gives a summary of literature on flow through tube banks.

Tube Arrangement	Source
Single Tube	**[69,70]**
Staggered	**[71,72]**
In-line	**[73,74,75,76]**
Staggered and In-line	**[39,77,78,79,80,81,82,83,84,85]**

Table 4-1 Literature Research Sources on Flow Around Tubes

These references will now be discussed in more detail.

4.1.2 Two-Phase Flow

The presence of solid particles in many industrial applications has a detrimental effect on the performance of the components. The problem of particulated flow in any flow system can be divided into three parts. The first part consists of the particle trajectories. The second is the effect of the presence of the particles on the fluid behaviour. The third part consists of the nature of the solid surface impact and the material erosion [**69**].

4.1.3 The Effect of Particles on Fluid Flow Properties

4.1.3.1 Around Tubes

The presence of particles in a fluid could affect flow properties such as streamline patterns, vorticity, coefficient of drag, separation angle, and recirculation eddies. With an increase in particle size, there is a larger difference in relative velocities between that of the particle and the air because of higher inertia, thus resulting in higher interphase forces. This leads to a change in the fluid velocities, resulting in an increased coefficient of drag of a tube in cross-flow. Thus, the influence of the particles on the fluid flow depends on the size and number of particles present for a given mass fraction. With an increase in particle mass fraction, the size of the recirculation zone increases. With larger-diameter particles, the length of the recirculation eddy is decreased with an increase in the particle concentration [**69**].

4.1.3.2 In the Rest of the Boiler

Gas flow patterns are determined primarily by the air inlet geometry and conditions are not greatly modified by liquor sprays and in-flight combustion [**86**].

4.1.4 Particle Rebound Phenomenon of Particles

The erosion of metals impacted by small dust particles as well as the rebound dynamics of these particles can only be described in a statistical sense [**34**,**40**]. This becomes obvious when one examines the number of geometric situations that might occur at impact [**34**]. Quartz sand was used in the research of Grant and Tabakoff[**34**]. The value of the velocity of a particle and the direction of its motion as it rebounds from the surface after collision must be known so that the solution of the particle equations of motion may be continued beyond the points of collision [**69**]. Equations (4-1) and (4-2) are the results obtained by Grant and Tabakoff[**34**].

$$\frac{V_{N_2}}{V_{N_1}} = 0.993 - 1.76\beta_1 - 1.56\beta_1^2 - 0.49\beta_1^3 \qquad (4\text{-}1)$$

$$\frac{V_{T_2}}{V_{T_1}} = 0.988 - 1.66\beta_1 + 2.22\beta_1^2 - 0.67\beta_1^3 \qquad (4\text{-}2)$$

The symbols of Equations (4-1) and (4-2) are defined in Figure 4-1.

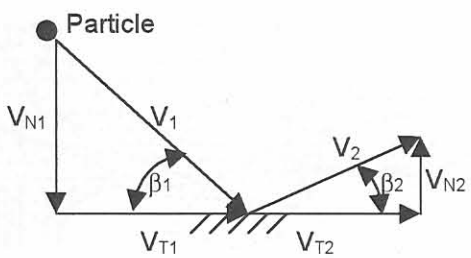

Figure 4-1 Velocity and Angle Notations for Particle Rebound Characteristics

4.1.5 Effect of particles size on particle trajectory in an in-line tube bank

Transverse and longitudinal tube spacing, cylinder diameter and the flow velocity of the gas seem to be important factors affecting particle trajectory, impact, and erosion when particle properties are fixed [**35**,**80**]. Two numerical simulations [**73**,**81**] are now discussed in more detail, as their results bear resemblance to the CFD simulation performed by the author to be presented later in this dissertation.

4.1.5.1 Numerical Simulation 1

This numerical simulation of two-phase flow in a tube bank was conducted by Jun and Tabakoff[**73**]. The flow and geometry specifications are as follows:

Flow Reynolds number (Re)	= 400 (Laminar)
Air density	= 1.23kg.m^{-3}
Particle size	= 40μm and 100μm
Particle density	= 2444kg.m^{-3} (sand); 1666kg.m^{-3} (Fly-ash)
Tube arrangement	= transverse- , longitudinal pitch = 2×cylinder diameter

Figure 4-2 shows the particle trajectories of 100μm sand. For these large particles, most of the rebounded particles from the first cylinder cross the mainstream and impact on the neighbouring cylinder surface either on the first or second row. Therefore a considerable amount of secondary impact occurs on the first cylinder surface either on the front side or on the backside relative to the main stream. Particles introduced in the wake do not change the direction significantly because the particle inertia is dominant compared to the aerodynamic forces acting on it. Impact occurs mostly on the front side of the first cylinder while it occurs less frequently on the front side of the second cylinder and on the backside of the first cylinder. According to the results from the simulation, the maximum erosion occurred at 40° to 70° from the leading edge, even though the maximum impact frequency occurred at 0° to 50° from the leading edge.

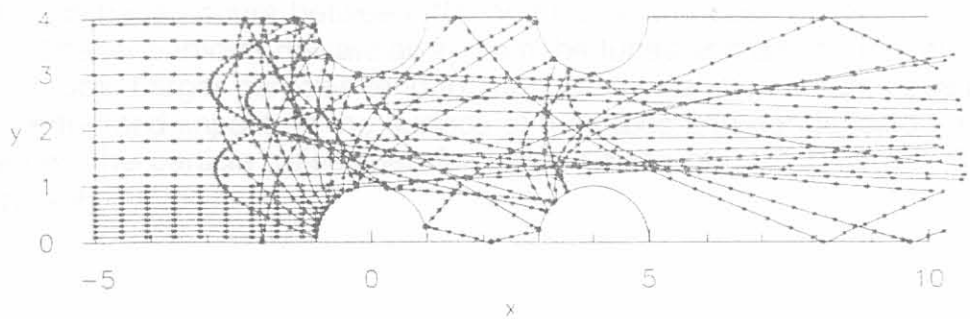

Figure 4-2 Particle Trajectories Over In-Line Tube Bank (Re=400); 100μm Sand [73]

Figure 4-3 shows the particle trajectories of 40μm fly-ash. For these smaller size particles, most of the impact on the first cylinders are primary impacts, while most of the impacts on the second cylinders are secondary impacts from the first row of cylinders. An interesting feature of the impacts on the second cylinders is that they are concentrated in a limited area on the tube surface in this particular case. The local maximum erosion on the second row of tubes occurs around 60° to 70° from the leading edge.

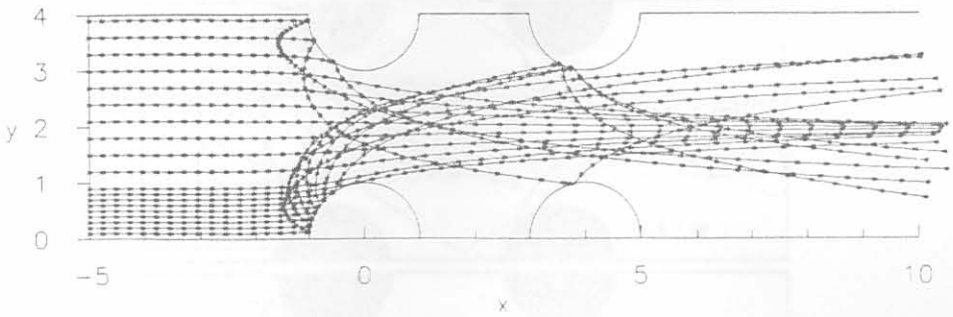

Figure 4-3 Particle Trajectories Over In-Line Tube Bank (Re=400); 40μm Fly-ash [73]

4.1.5.2 Numerical Simulation 2

This numerical simulation of two-phase flow in a tube bank was conducted by Fan et al.[**82**]. The simulation properties are as follows:

Particle material	= coal ash
Gas velocity	= 6.1m.s^{-1}
Air density	= 1.23kg.m^{-3}
Particle size	= 20, 30, 40, 50, 100, 200μm
Particle density	= 2450kg.m^{-3}
Tube arrangement	= transverse-, longitudinal pitch = 2×cylinder diameter

Erosion damage occurs between 40° and 60° in the case of the first row of tubes. Smaller particles deviate away from the tubes and do not impact on the tube surface. Larger particles tend to keep their initial momentum because of their inertia, and impact on the surface of the tubes and get deflected. Figure 4-4 shows the particle trajectories for particle sizes of 0.02, 0.05 and 0.1mm respectively.

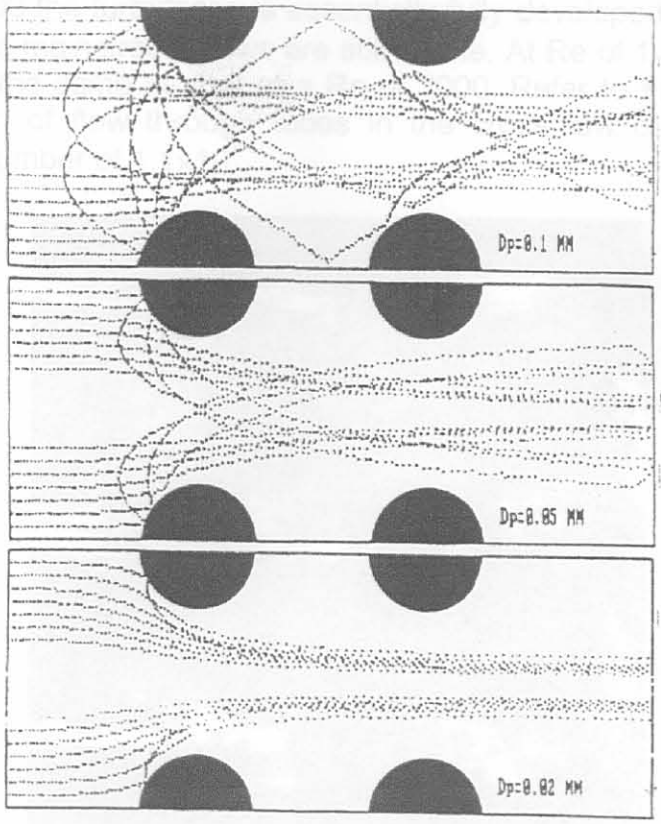

Figure 4-4 Particle Trajectories in Two-Phase Flow Around In-Line Tubes (V_∞=10m/s) [82]

4.1.6 Observations of Flow Phenomena in an In-Line Tube Bank

Here are some observations made by other researchers regarding flow phenomena in in-line tube banks:

- Fujii and Fujii[**74**] found that an almost fully-developed flow pattern is attained behind the first row of tubes. Weaver and Abd-Rabbo[**75**] observed flow patterns for an in-line array of four tube rows over a wide range of Reynolds numbers. Flow visualisation showed that the flow development is a function of not only Reynolds number but also of the row number of tubes.
- From pressure drop experiments conducted by Traub[**84**], it follows that the drag coefficient is almost independent of the inlet turbulent intensity over a wide range of Reynolds numbers.
- Flow visualisation by Weaver and Abd-Rabbo[**75**] shows that the flow pattern around the first and second row tubes is not typical of that around the third and subsequent rows. For Re = 30, the wake regions between the tubes appears essentially stagnant. As Re is increased, the wakes are seen to consist of two stable vortices with clear straight flow lanes between the columns. At a Re of about 150, these vortices begin to become unstable, with the flow crossing the wake region and the vortices periodically being swept into the mainstream flows. There is no evidence that the mainstream flow is significantly affected by the developing turbulence in the wakes. At Re = 400, the wakes become fully turbulent. At

a Re of 3000 the turbulence is essentially fully developed by the third row although the mainstream flows are still visible. At Re of 1.1×10^4 the flow is essentially the same as that at a Re of 3000. Refer to Figure 4-5 for the visualisation of flow through tubes in the cross-flow configuration at a Reynolds number of 1.1×10^4.

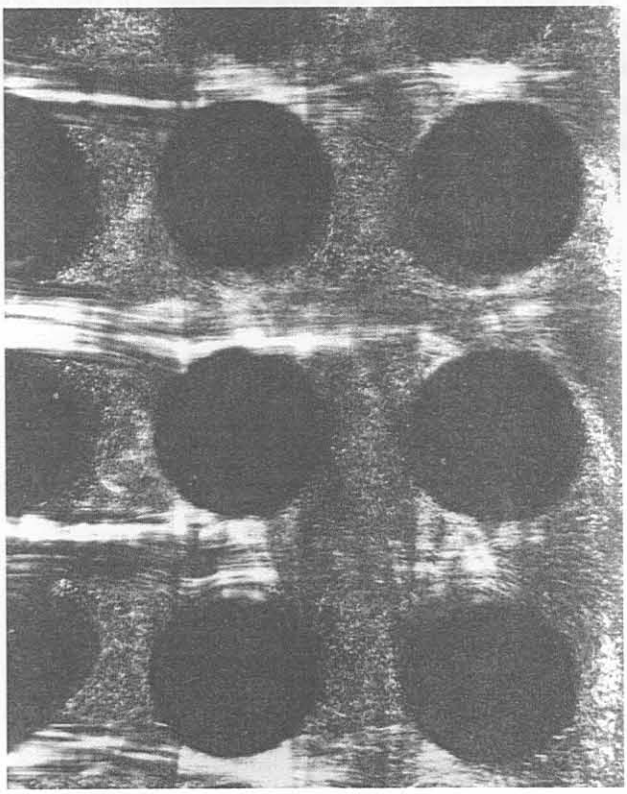

Figure 4-5 Flow Visualisation in an In-Line Tube Bank (Re=1.1×10^4) [75]

- The flow is steady at the entrance of the tube banks, but becomes oscillatory downstream of the onset location of vortex shedding [**79**].
- Tube erosion damage by particle impaction depends on the particle size and the free stream velocity [**72**].
- Flow visualisation by Nishimura et al.[**78**] shows that the flow changes from steady to unsteady at about Re=100 due to vortex shedding for in-line as well as staggered tube arrays.

4.1.7 The Effect of a Gap Between Tube Rows of an In-Line Tube Bank

Gaps between adjacent layers of crossflow in-line tube banks are sometimes required because of manufacturing feasibility or soot blowing lanes. Only one paper could be found that deals with the effect of a gap between rows of an in-line tube bank. Zhang and Chen[**87**] did research on how a gap influences heat transfer of tubes in a tube bank. No literature was found however that deals exclusively with erosion or flow patterns in a tube bank with a gap between adjacent tube rows. Zhang and Chen[**87**] found that the existence of

a gap enhanced the heat transfer of those tubes just adjacent to the gap by 10 to 30%.

4.1.8 Conclusion

Particles can affect flow in tube banks but do not influence large-scale boiler flows. Two-phase flow in in-line tube banks is dependent on tube spacing as well as particle size. Smaller particles do not impact tubes in tube banks, as do larger particles. It was also discovered that flow in in-line tube banks is fully turbulent at a Reynolds number of 3000 and the flow field remains essentially the same for larger Reynolds numbers.

4.2 CFD Modelling of Erosion and Boiler Flow

4.2.1 Introduction

There are a few papers available in the literature on erosion in boilers and the nature of flow through the boiler using CFD. Because CFD will be used in this study, it is important to know what other researchers had done, what assumptions they made and how accurate their results were compared to measurements.

4.2.2 Boundary Conditions, Heat Transfer and Two-Phase Flow

As already discussed in Chapter 2, is it important to apply the correct boundary conditions to obtain realistic results.

4.2.2.1 Inlet Boundary Conditions

The following assumptions were made by other researchers regarding boiler inlet conditions:

- In all the research found on CFD simulation of flow through a boiler, a uniform inlet flow velocity profile and geometry was assumed [**48**,**88**,**89**,**90**,**91**]. Figure 4-6 illustrates an example of a uniform velocity inlet as applied to boiler CFD models.
- Shen et al.[**89**] also assumed a uniform inlet temperature distribution.
- Tu et al.[**48**] assumed a uniform inlet fly-ash concentration distribution.
- Inlet turbulence intensity is taken to be 5% by Tu and Fletcher[**88**], and 10% by Shen et al.[**89**].

The following conclusions were drawn from studies by other researchers regarding boiler inlet conditions.

- Shen et al.[**89**] concluded during upper boiler studies that different inlet velocity and temperature profiles do not significantly alter the velocity field and temperature distributions through a boiler.
- Vakkilainen et al.[**91**] used a variety of inlet velocity profiles and temperature profiles to determine the sensitivity of the results to chosen inlet conditions. Results from this work show that predicted temperature profiles and velocity profiles at the boiler bank and superheater heat transfer surfaces were not affected significantly by these inlet conditions. Flow features like channelled flow, tangential swirling and recirculation zones can be very strong in the lower furnace near the air jets, but dissipate somewhat due to turbulent shear in the upper furnace.

4.2.2.2 Outlet Boundary Conditions, Heat Transfer and Ash Particles

This section describes some assumptions made or conclusions reached by other researchers regarding boiler outlet conditions, heat transfer and ash particles in simulated boiler environments.

- The normal gradient of all dependent variables is set to zero at the outlet of the computational domain [**48**,**88**].
- Shen et al.[**89**] found that radiation heat transfer in boilers can be omitted in CFD simulations without influencing flow patterns through the boiler.

- The solid particles are assumed to have no influence on the gas flow [**89**].
- Fly-ash particles are assumed to be spherical [**48**].

4.2.3 Computational Grids

As discussed in Chapter 2.5, the grid must be of an appropriate quality to obtain reliable CFD results. The rest of this section gives a summary of grid sizes used by other researchers. An example of a computational grid is also illustrated. This information will give guidelines of what grid are required in boiler CFD models.

- Shen et al.[**89**] used 50 410 cells (71×71×10) in the CFD model. The geometry of the computational domain can be seen in Figure 4-6.

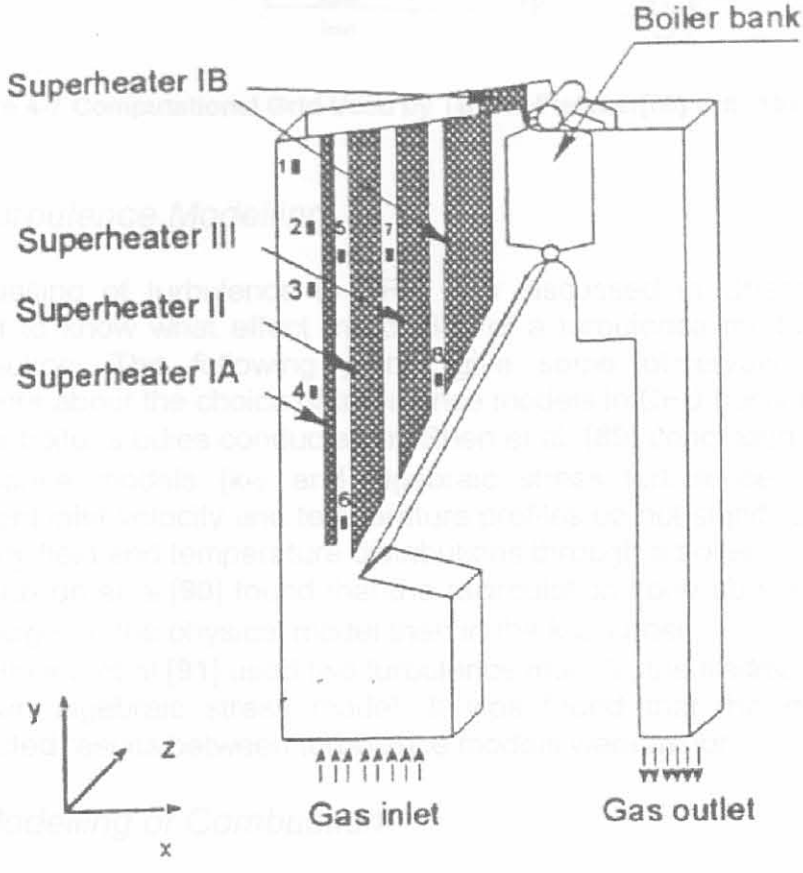

Figure 4-6 Schematic of Modelling Geometry used by Shen et al.[89]

- Tu et al.[**48**] used 117000 cells (30×130×30) in a domain almost similar to the one illustrated in Figure 4-7.
- Vakkilainen et al.[**90**] used 21888 cells (32×36×19) extending from below the bullnose to the exit of the boiler bank.
- Vakkilainen et al.[**91**] used 50000 nodes extending from below the bullnose to the entrance of the economiser.
- Tu and Fletcher[**88**] used a grid of 103168 cells (62×52×32). This grid is shown in Figure 4-7.

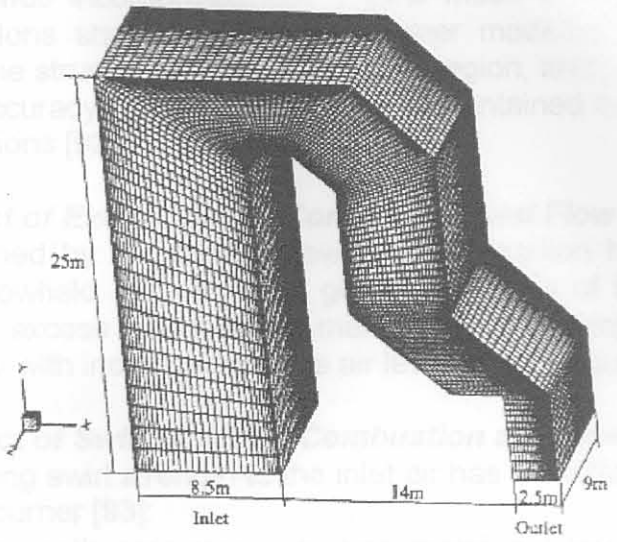

Figure 4-7 Computational Grid Used by Tu and Fletcher[88] with 103 168 cells

4.2.4 Turbulence Modelling

The modelling of turbulence in CFD was discussed in Chapter 2.3. It is important to know what effect the choice of a turbulence model has on the CFD solution. The following points give some observations by other researchers about the choice of turbulence models in CFD boiler models.

- Upper boiler studies conducted by Shen et al. [**89**] concluded that different turbulence models (k-ε and algebraic stress turbulence models) and different inlet velocity and temperature profiles do not significantly alter the velocity field and temperature distributions through a boiler.
- Vakkilainen et al.[**90**] found that the recirculation zone above the bullnose was larger in the physical model than in the k-ε model.
- Vakkilainen et al.[**91**] used two turbulence models, the traditional k-ε model and an algebraic stress model. It was found that the differences in predicted results between turbulence models were minor.

4.2.5 Modelling of Combustion

Because the modelling of combustion is very complex as will become evident in the rest of this section, ways must be investigated to simplify the modelling of combustion and what effect this simplification will have on the flow field through a boiler.

Grace et al.[**86**] found that gas flow patterns are determined primarily by the air inlet geometry and conditions, and are not greatly modified by liquor sprays and in-flight combustion.

4.2.5.1 Burner Modelling

The CFD solver STAR-CD has been used successfully by other researchers to assess NOx production and char burnout trends in boilers. A detailed

burner geometry was incorporated into a CFD mesh of 420000 cells. The STAR-CD predictions show that detailed burner modelling is essential to reproduce the flame structure in the near-burner region, and provided that this is done, a high accuracy of predictions can be maintained in the scale-up to multiburner conditions [**92**].

4.2.5.2 The Effect of Excess Air on Combustion and Flow

The results obtained by Gupta[**93**] show that combustion has a significant effect upon the flowfield. Although the general features of the flowfield are unaffected by the excess air level, the maximum mean temperatures decay much more rapidly with increased excess air level than its counterpart.

4.2.5.3 The Effect of Swirl of Air on Combustion and Flow

The effect of varying swirl strength to the inlet air has the following features of the flow near the burner [**93**]:

- Higher swirl strength promotes a higher centrifugal force, and hence a larger central recirculation zone core diameter.
- Increased swirl strength reduces or eliminates the size of the corner recirculation zone and increases the central toroidal recirculation zone.
- Combustion reduces the length and width of the central recirculation zone, under similar conditions of swirl to the airflow.

4.2.6 Other Observations of Flow through Boilers using CFD

4.2.6.1 The Effect of the Tube Bank on Flow through the Boiler

The points discussed next are observations and assumptions made by other researchers on the effects of the tube bank on the flow pattern through the boiler.

- If the tube bank is not included in the CFD model, the channelled flow narrows at the exit of the superheater and the temperatures in the recirculation zone are moderately higher. In addition, if the flue gas is assumed to have a constant density, the temperatures in the recirculation are moderately lower [**89**]. Shen et al.[**89**] treated the tube bank as a lumped heat exchanger with non-isotropical heat transfer coefficients and pressure loss coefficients.
- Tu et al.[**48**] showed that it is possible to obtain a good indication of regions of high erosion rate without the need of modelling tube banks, thus greatly simplifying the calculations. The quality of the solutions in boilers without tube banks is sufficient to provide an insight into the flow phenomena and erosion patterns within coal-fired boilers.
- Vakkilainen et al.[**90**] concluded that the modelling of flow without boiler internals such as the superheater tubes and tube bank give better results for the flow field through the boiler than models with internals, where the tube bank was modelled using a porous cell approximation.

4.2.6.2 The Effect of the Bullnose on Flow through the Boiler

The purpose of the bullnose is to protect the superheater tubes from furnace radiation [**90**]. The design of the upper boiler and the shape of the bullnose result in a large recirculating flow above the bullnose which greatly reduces the convective heat transfer [**89**,**90**]. It was found, however, that the velocity

and temperature distributions are sensitive to the shape and size of the bullnose [**89**]. The effect of size and shape of the bullnose on gas temperature and velocity were investigated for three sizes and three shapes by Vakkilainen et al.[**91**]. Both the size and the shape of the bullnose affected gas flow.

4.2.6.3 Inertia of Particles

Here are some observations made by other researchers regarding particles in boiler flows through the use of CFD.

- The flue gas and fly-ash entrained into the economiser are thrown to the rear wall of the economiser due to centrifugal forces. The velocities of both flue gas and fly ash are highest in this region [**48**].
- Smaller fly-ash particles are more influenced by the gas flow, and, with increasing particle size, the larger particles are accelerated by the centrifugal force and flung outwards [**88**].

4.2.7 Conclusion

CFD has previously been used by researchers to model erosive boiler environments with success. Good results can be obtained with assumptions such as uniform inlet velocity and temperature profiles. Radiation can also be omitted in CFD boiler simulations without affecting the flow pattern through the boiler significantly. Combustion can therefore be ignored in CFD models for upper boiler erosion studies. Boiler internals, such as the tube bank, do not have to be modelled to indicate regions of high erosion rate. The effect of the turbulence model used in boiler flows has a negligible effect on the flow field apart from small changes in the sizes of recirculation zones. From all the information gathered in this section, it becomes obvious that great simplifications can be made to boiler CFD models.

4.3 CFD Analysis : A Parametric Study for Different Conditions of Flow Through a Boiler

4.3.1 Introduction

The following section is a parametric study of the influence that certain parameters like inlet velocity, inlet geometry and porosity of boiler internals have on the flow field through the boiler. The effect of particle size on particle trajectories is also investigated. This section of this study does not simulate real boiler operating conditions of the Babcock boilers but it is done to become familiar with boiler flows and to see the effect of different parameters on the flow field through the boiler.

4.3.2 2D Analysis of the Boiler

The first CFD analysis of the boiler is a 2D simulation of the flow through the boiler. A 2D grid is used because it produces fast results and should be efficient to visualise the flow field through the boiler. The 2D simulation is a very useful first analysis.

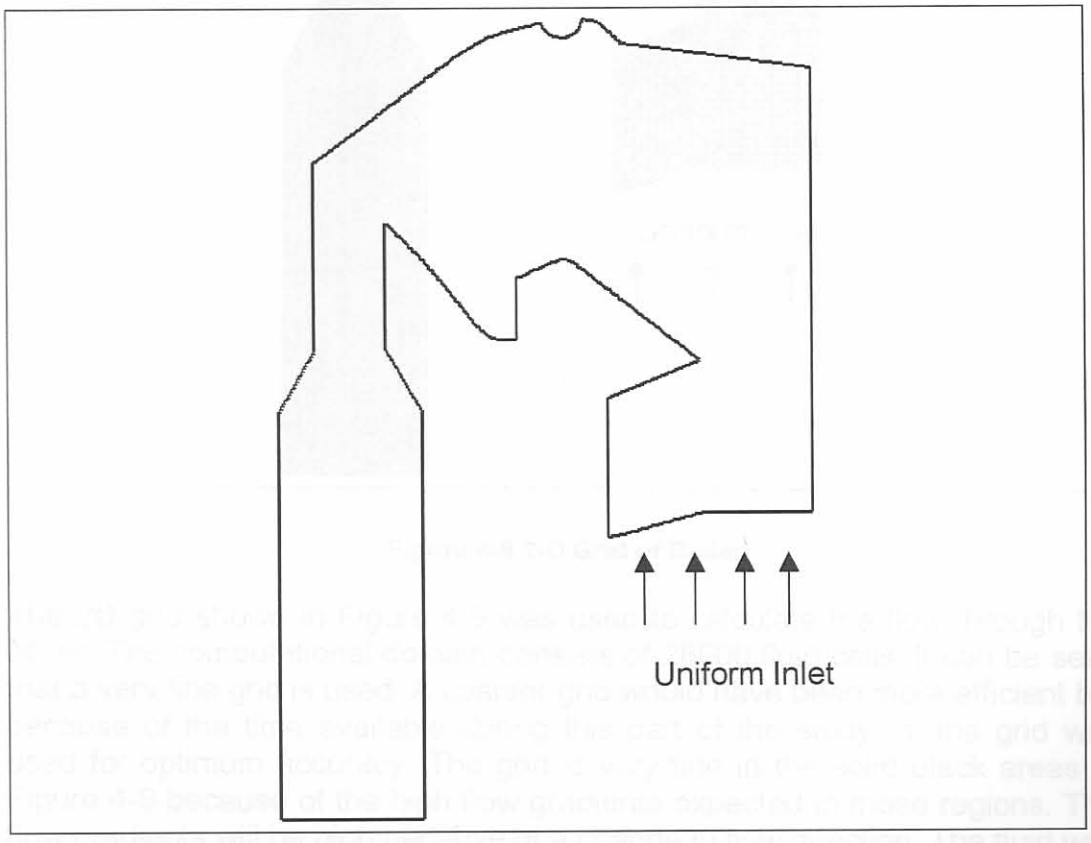

Figure 4-8 Edge Plot of 2-Dimensional Boiler Geometry

Figure 4-8 shows the outline of the boiler that is used for the 2D CFD simulation. A uniform inlet geometry and velocity distribution below the bullnose and a outlet boundary after the airheater are used as was used by

Tu et al.[**48**], Tu and Fletcher[**88**], Shen et al.[**89**] and Vakkilainen et al.[**90**,**91**].

4.3.2.1 The Effect of Inlet Velocity on the Flow

To interpret CFD results it is vital to do a sensitivity analysis of boiler flows to certain boiler operating parameters. If the flow pattern through the boiler doesn't change much when the inlet velocity is changed, for example, one knows that the flow field in the boiler is relatively stable and would not change if other inlet conditions were used. The solution is then Re-number independent.

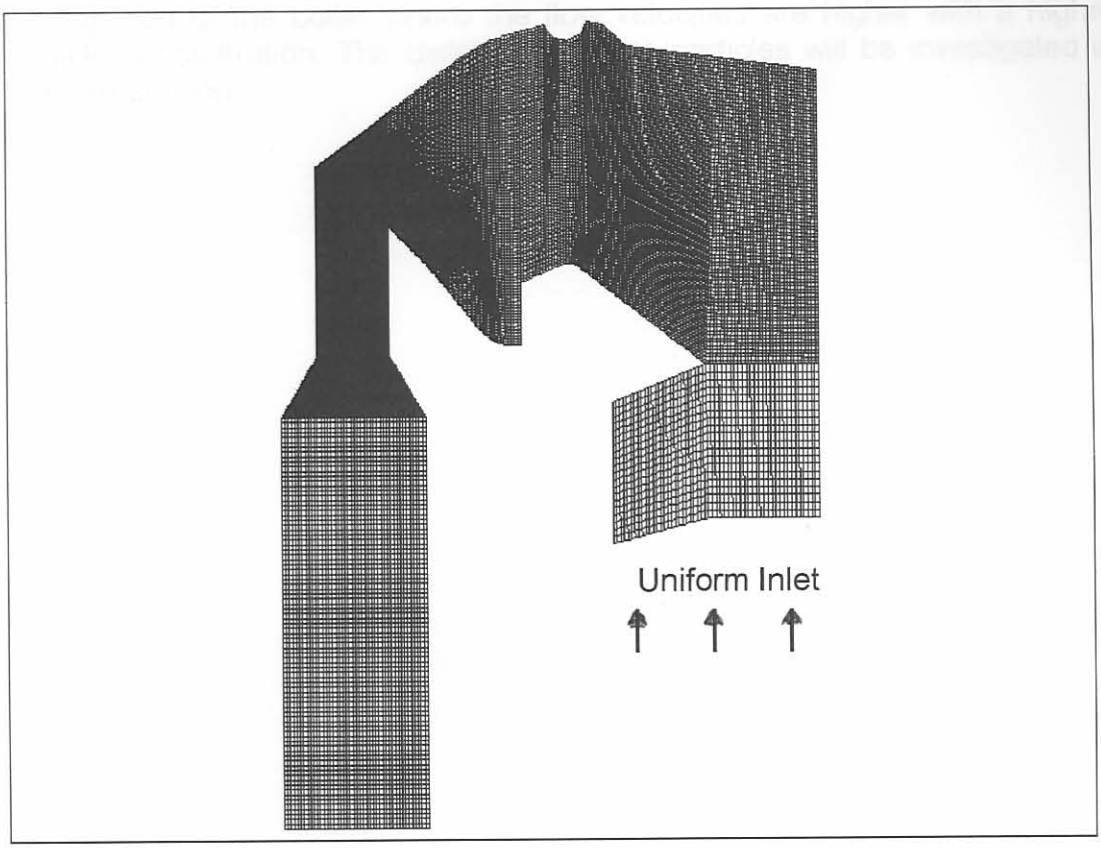

Figure 4-9 2-D Grid of Boiler

The 2D grid shown in Figure 4-9 was used to calculate the flow through the boiler. The computational domain consists of 28000 fluid cells. It can be seen that a very fine grid is used. A coarser grid would have been more efficient but because of the time available during this part of the study, a fine grid was used for optimum accuracy. The grid is very fine in the solid black areas of Figure 4-9 because of the high flow gradients expected in those regions. The flow gradients will be high because of a change in flow direction. The fluid was simulated as incompressible air with no heat transfer. The turbulent model used was the k-ε model.

Figure 4-10 and Figure 4-11 illustrate the flow fields for the different inlet velocities. Only plots of velocity magnitude are shown because velocity is one of the most important parameters influencing erosion [**24**,**26**]. It can be seen

that the flow fields are exactly the same for the two different input velocities. Inlet velocity is thus not an important factor when determining where the areas of localized high velocity are. As expected, there is a major recirculation zone above the bullnose that extends from the tip of the bullnose to the inlet passage of the airheater. Only the top half of the tube bank therefore transfers heat efficiently. This is consistent with the findings of Shen et al.[89] and Vakkilainen et al.[90].

Erosion is a direct consequence of the flow pattern caused by the shape and size of the bullnose. The bullnose causes the large recirculation zone and the flow is therefore not uniform across the tube bank. There is channeled flow in the top part of the boiler where the flow velocities are higher with a higher particle concentration. The distribution of the particles will be investigated in the next section.

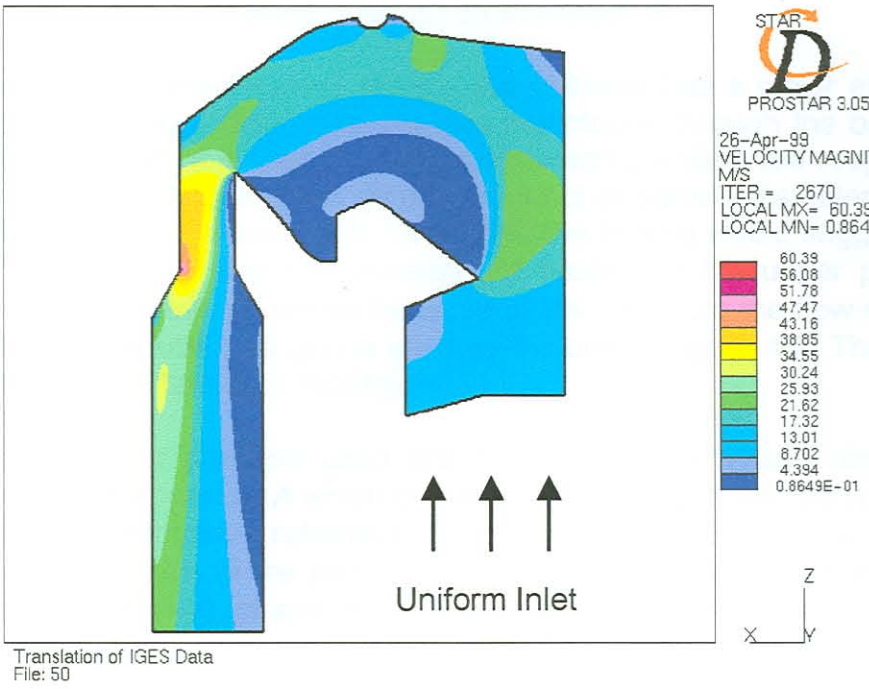

Figure 4-10 Velocity Magnitude Plot (10m.s^{-1} at Inlet)

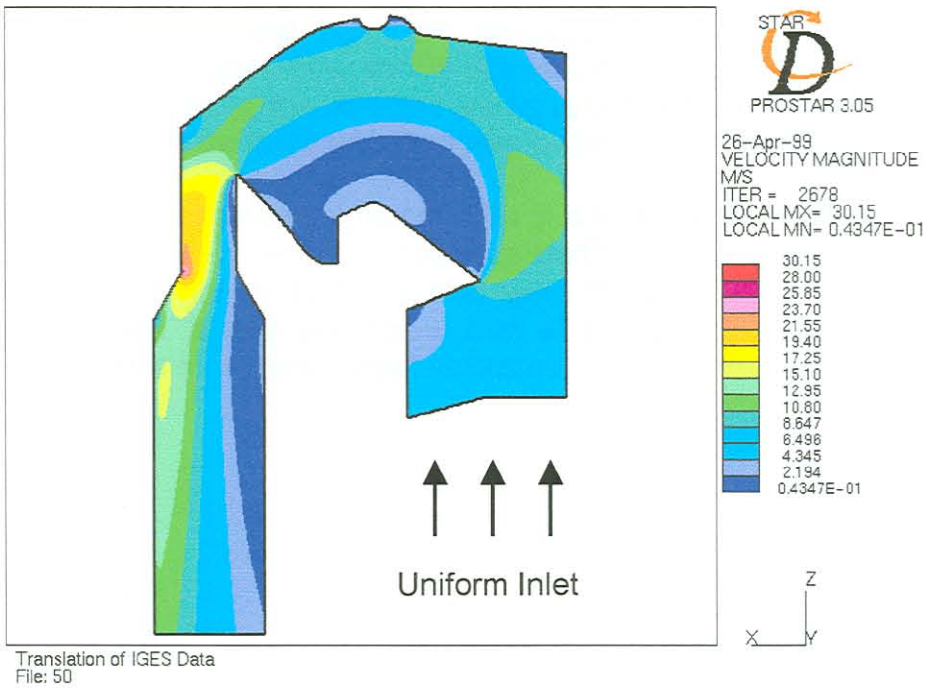

Figure 4-11 Velocity Magnitude Plot (5m.s^{-1} at Inlet)

4.3.2.2 Particle Trajectories for 2D Boiler Models

As discussed in the previous section the bullnose has a major effect on the flow pattern through the boiler. Particle trajectories through the boiler will be investigated next. It is important to know which particles are responsible for material loss through erosive wear. The effect of particle diameter on particle trajectories is also investigated. One's intuitive feeling would suggest that the larger particles are more responsible for erosion in the upper parts of the boiler due to centrifugal forces because of the 180° turn the flow must follow. The same computational grid is used as the one in Figure 4-9. The density of the particles are taken as 1650kg.m^{-3}.

The diameter of particles used are 10 and 100μm. These diameters are obtained from Appendix A which contains the analysis of ash particle diameter for fly-ash samples retrieved from the Babcock boilers at Sasol. Approximately 10% of the particles are 10μm and smaller and about 10% of the particles are 100μm and larger. The bulk of ash diameters are between 10 and 100μm.

Figure 4-12 to Figure 4-15 show the particle trajectories for 10 and 100μm particles for 10 and 5m.s^{-1} inlet velocities respectively. It can be seen that the smaller particles follow the gas streamlines, whereas the larger particles are flung outwards due to centrifugal forces.

The 10μm particles follow almost exactly the same trajectories for both the 5m.s^{-1} and 10m.s^{-1} inlet boundary conditions. For the 100μm particles, however, the trajectories differ for the different inlet conditions. For the case of the higher inlet velocity, the particles are flung outwards towards the top of the boiler more than is the case with the lower boiler inlet velocity.

This results are in agreement those of Tu and Fletcher[**88**]. The particle sizes used by Tu and Fletcher[**88**] to calculate particle trajectories are between 5 and 150μm. The larger particles also were flung outwards more than the smaller particles. It was also found that all the particles follow almost the same trajectories for different input velocities.

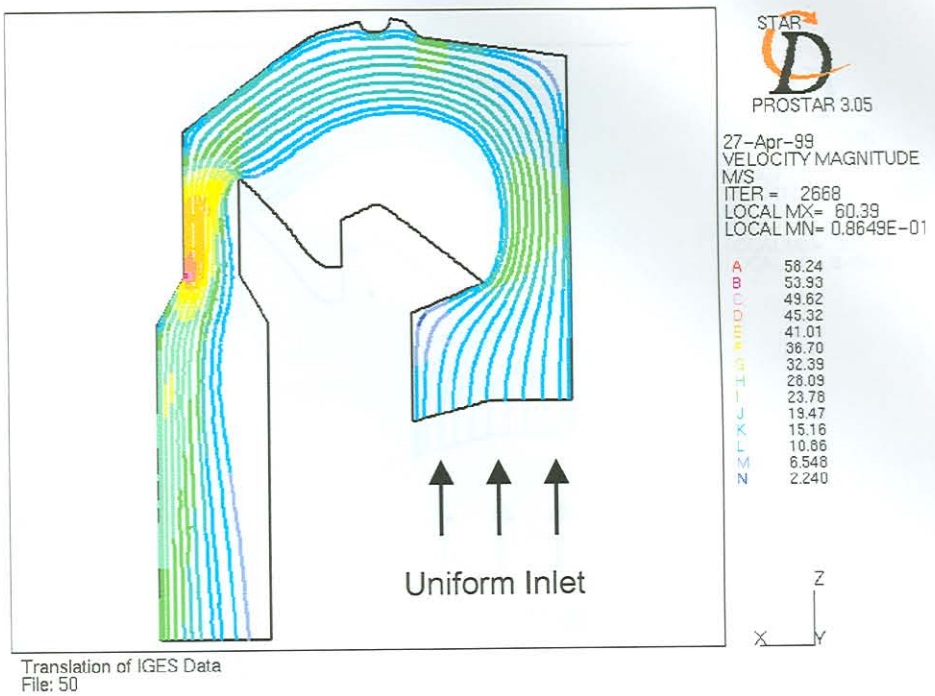

Figure 4-12 Particle Trajectories for 10μm Particles (10 m.s^{-1} Uniform Inlet)

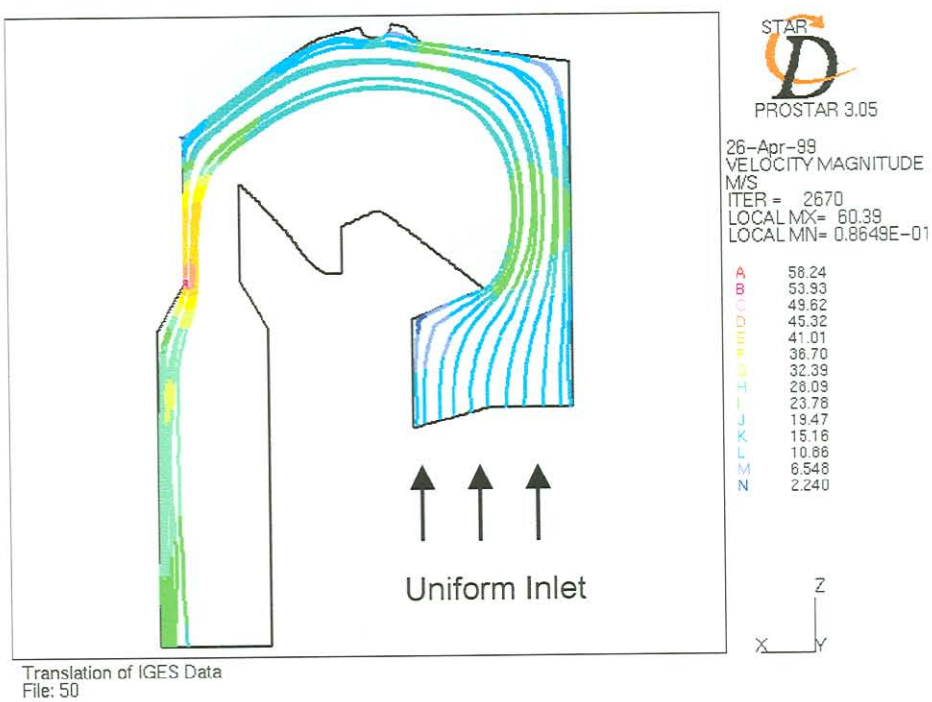

Figure 4-13 Particle Trajectories for 100μm Particles (10m.s^{-1} Uniform Inlet)

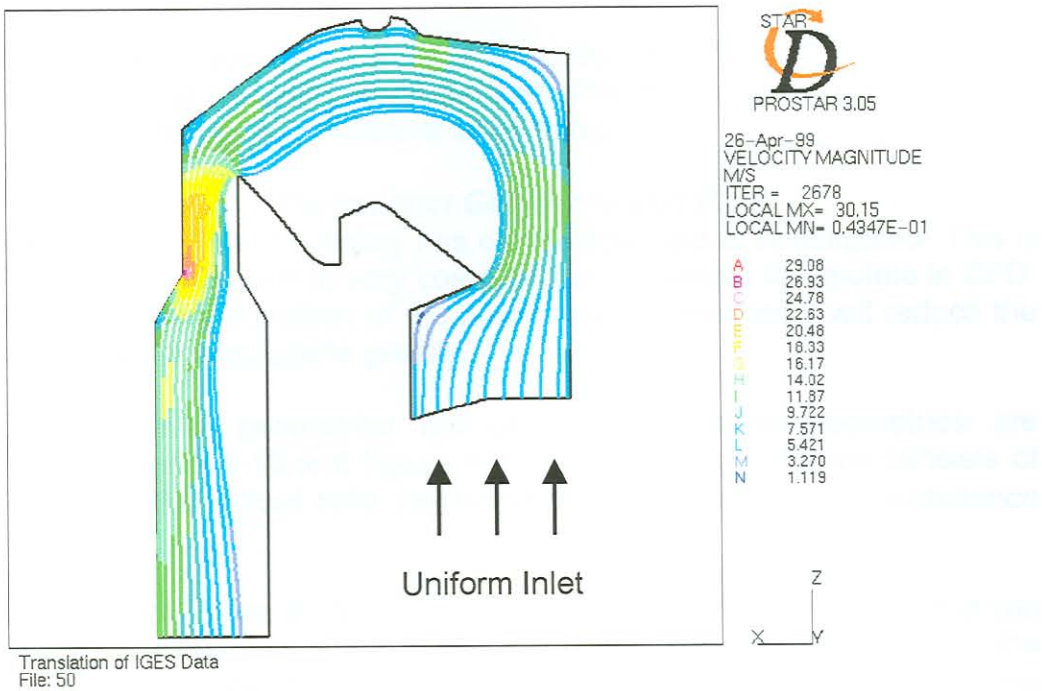

Figure 4-14 Particle Trajectories for 10μm Particles (5 m.s^{-1} Uniform Inlet)

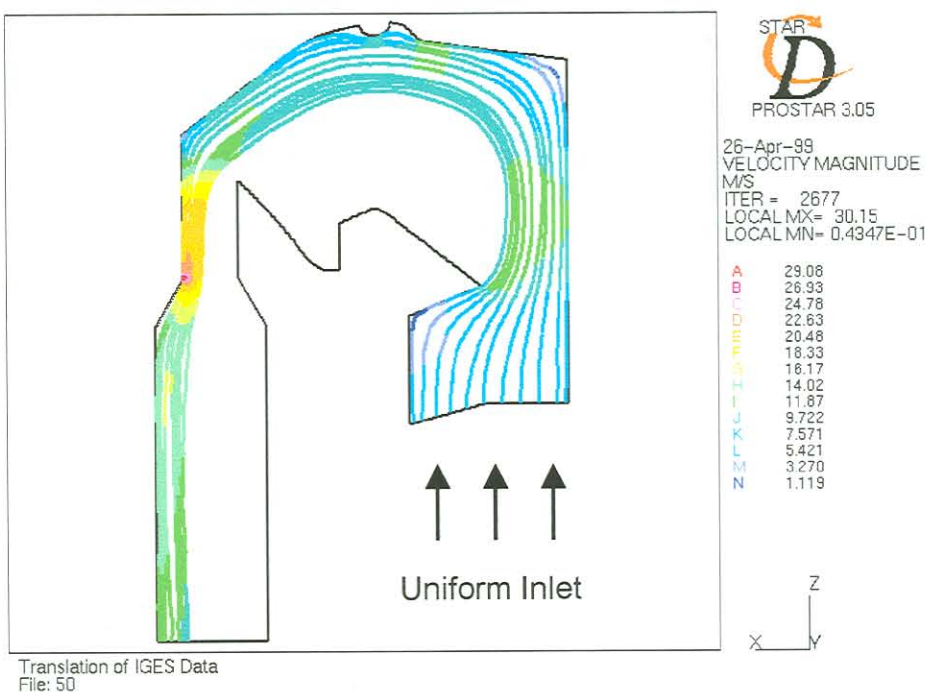

Figure 4-15 Particle Trajectories for 100μm Particles (5m.s^{-1} Uniform Inlet)

4.3.3 3D Analysis of the Boiler

In the previous section the boiler was simplified to only a 2D model. In this section a 3D boiler geometry is considered. The differences between 2D and 3D CFD boiler models can therefore be investigated.

4.3.3.1 The Effect of Different Inlet Geometries on Flow

The effect that the inlet boundary has on the flow field is investigated. This is done because combustion is very complex and expensive to simulate in CFD. If the inlet boundary condition of the boiler can be simplified it will reduce the cost of CFD boiler simulations greatly.

Two different inlet geometries are used. These boiler geometries are illustrated in Figure 4-16 and Figure 4-17. These two geometries consists of 186324 and 243296 fluid cells respectively. Once again the k-ε turbulence model is used.

Figure 4-18 and Figure 4-19 show the velocity magnitude plots for the two different boiler inlet geometries at the symmetry plane of the boiler for the same volume flow rate through the boiler. The only major differences in the flow fields are in the radiation chamber below the bullnose, which is obviously due to the different inlet geometries. The flow fields in the upper boiler, above the bullnose, are nearly the same. The recirculation zone above the bullnose for both cases has nearly the same shape and size. When these results are compared to the 2D results of the previous section, it is clear that there are no great differences in the flow patterns for the different dimensional CFD models.

Shen et al.[**89**] found that the inlet velocity and temperature profiles do not significantly alter the velocity field distribution through a boiler. Vakkilainen et al.[**91**] also used different inlet conditions and it was concluded that flow features like channelled flow, tangential swirling and recirculation zones can be very strong in the lower furnace near the air jets, but dissipate due to turbulent shear in the upper furnace. The results obtained in this section are thus in good agreement with other researchers' findings.

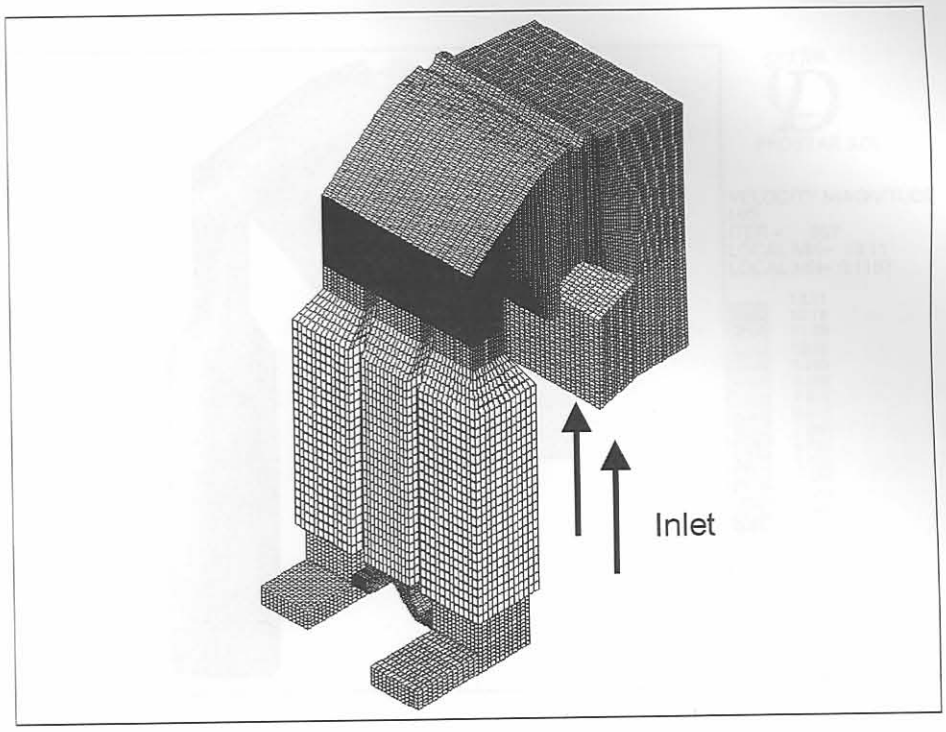

Figure 4-16 3-D Computational Grid with Uniform Inlet

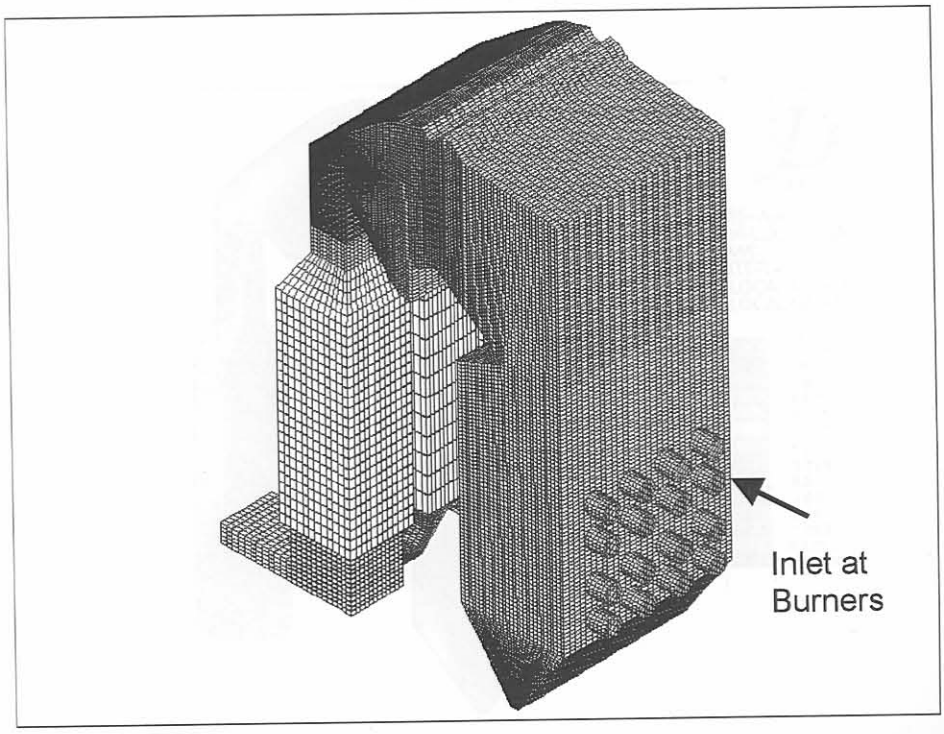

Figure 4-17 3-D Computational Grid with Inlet at Burners

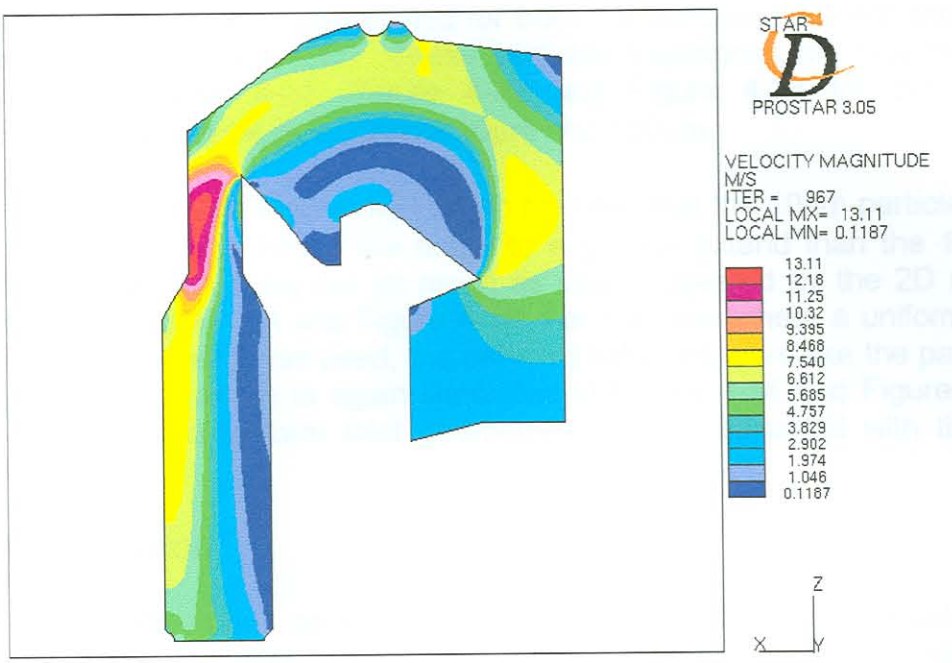

Figure 4-18 Centreline Velocity Magnitude Plot with Uniform Inlet (Mass flow rate of 216.59kg.s^{-1})

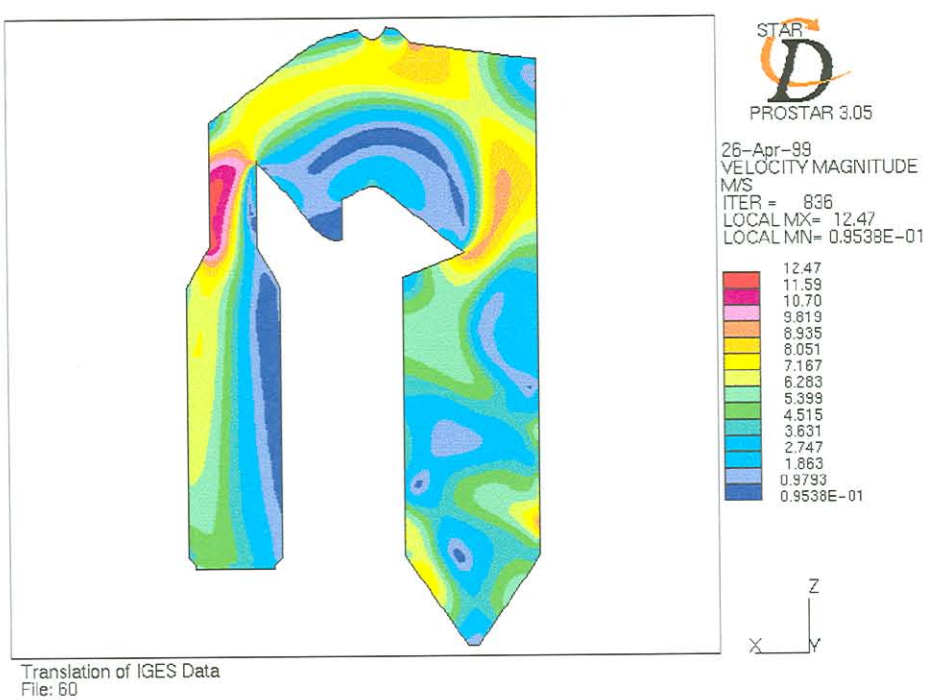

Figure 4-19 Centreline Velocity Magnitude Plot with Inlet at Burners (No Swirl) (Mass flow rate of 216.59kg.s^{-1})

4.3.3.2 Particle Trajectories for 3D Boiler Models

Particle trajectories were determined for both the 3D boiler models shown in Figure 4-16 and Figure 4-17. These particles trajectories are illustrated in Figure 4-20, Figure 4-21, Figure 4-22 and Figure 4-23 for both inlet geometries and particle diameters of 10μm and 100μm.

From Figure 4-20 and Figure 4-21 it can be seen that the 10μm particles are flung outwards to the top of the boiler to a greater extend than the 100μm particles. It was not flung out as much as was suggested by the 2D model illustrated in Figure 4-14 and Figure 4-15. For the case where a uniform inlet velocity and geometry was used, the particles behaved more like the particles of the 2D model, which is again illustrated in Figure 4-14 and Figure 4-15. This is because a uniform inlet geometry was also assumed with the 2D model.

4.3.4 Conclusion

From the results in this section, it can be seen that different inlet velocities does not in any way alter the flow field through the boiler. It can therefore be assumed that the flow field will remain approximately the same for other inlet velocities. If different inlet geometries are used in 3D CFD models, the flow fields are approximately the same in the upper boiler above the bullnose. It was also found that the flow fields do not differ much for 2D and 3D models in the centre plane of the boiler. It is expected though that the flow field will differ near the boiler walls. In both 2D and 3D models, the trajectories of particles behave the same for 10μm and 100μm particles. The 10μm particles follow the streamlines of the flow while the 100μm particles are flung outwards towards the top of the boiler due to centrifugal forces.

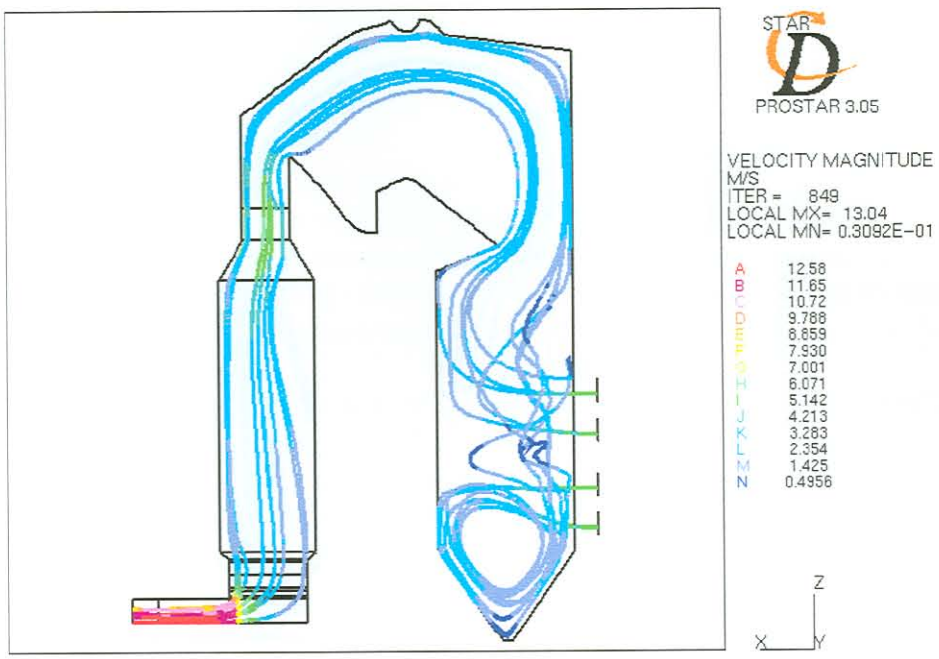

Figure 4-20 Particle Trajectories for 10μm Particles

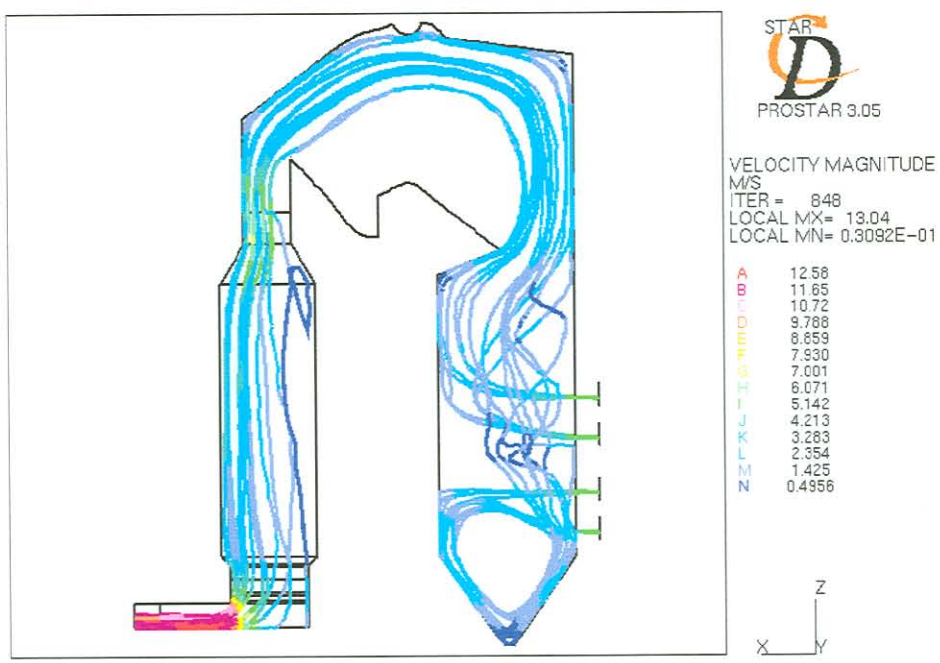

Figure 4-21 Particle Trajectories for 100μm Particles

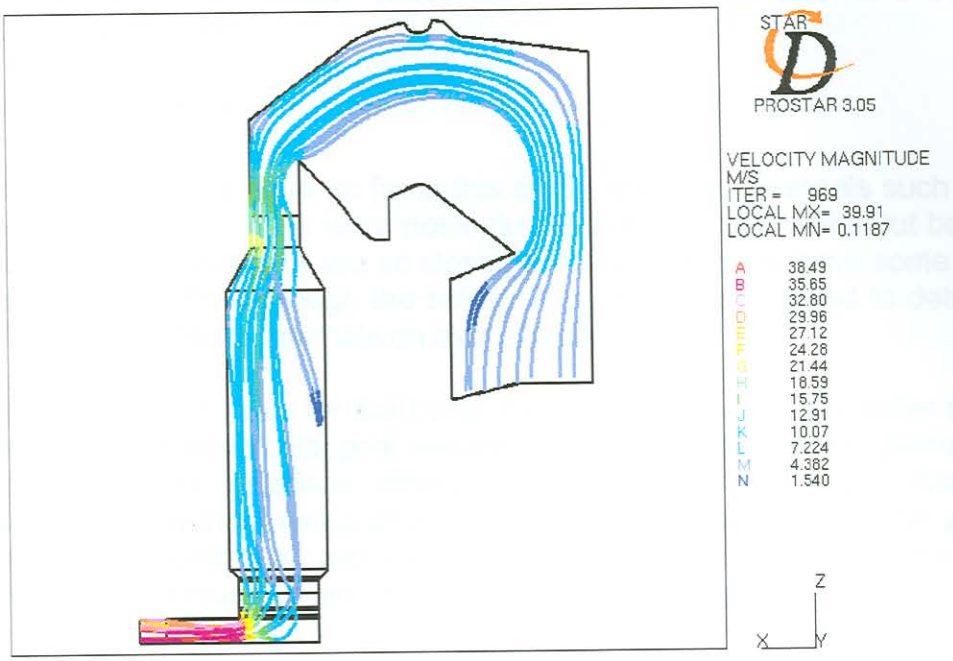

Figure 4-22 Particle Trajectories for 10μm Particles

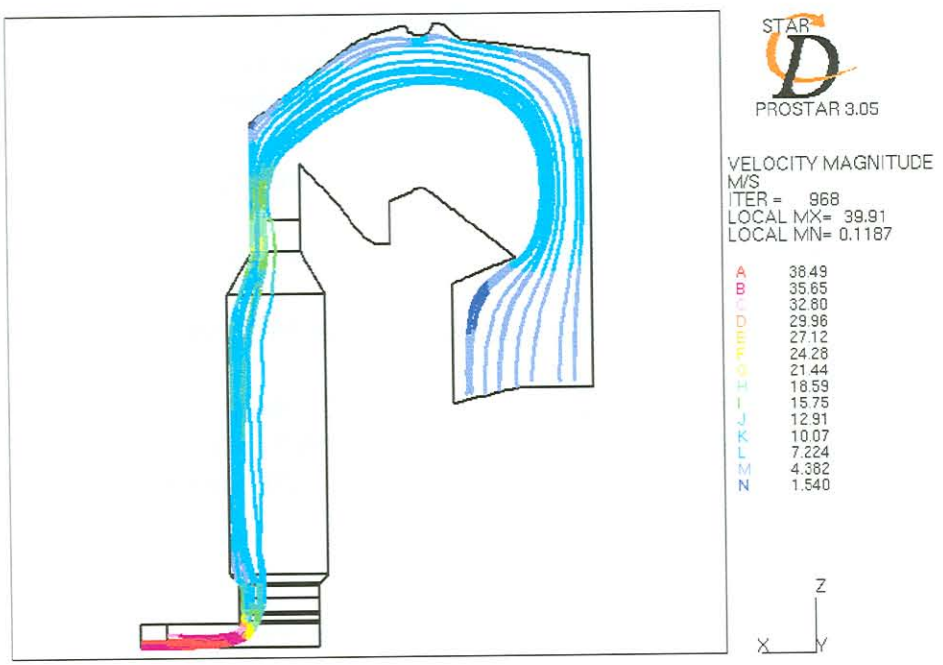

Figure 4-23 Particle Trajectories for 100μm Particles

4.4 Modelling of Boiler Internals through the use of Porosity Coefficients

4.4.1 Introduction

In the CFD analyses done so far in this study, the boiler internals such as the airheaters and boiler bank were not included in the CFD models. But because the tubes of the tube bank are so closely packed, they must have some sort of influence on the flow through the boiler. This section is devoted to determine the effect of the boiler internals on overall boiler flows.

It is not feasible to solve for the boiler internals directly in CFD boiler models because of the fine-scale grid required near the boiler tubes. Because of computer memory limitations, alternative methods must be used to model the boiler internals without using small-scale grids. This is done through the use of porous sections that replace the boiler internals, but have the same pressure drop versus velocity characteristics as the tubes they replace.

One usually uses porous cells in a CFD code if there exists fine-scale geometrical structures in a flow field. The effect of these structures is usually too small to resolve numerically within the overall calculation. Examples of these include[**3**]:

- Flows in porous media, such as packed-bed chemical reactors.
- Heat exchangers of the shell-and-tube type, where the calculation is to encompass the entire assembly, containing a large number of tubes/plates. (In this study the porous cells are used for this reason.)
- Flows in fibrous materials.
- Filters.
- Honeycomb structures.

In this study porous sections are used to replace the tube banks of the boiler.

4.4.2 Calculation of Porosity Coefficients

The assumption is made that everywhere within the volume containing the distributed resistance, there exists a local balance between pressure and resistance forces such that:

$$-K_i \cdot u_i = \partial p / \partial \xi_i \qquad (4\text{-}3)$$

Where:

$\xi_{i.}$ ≡ Orthotropic directions (i. = 1,2,3)
K_i ≡ Permeability
u_i ≡ Superficial velocity in direction $\xi_{i.}$

The permeability K_i is assumed to be a quasilinear function of the superficial velocity magnitude $/v/$ of the form:

$$K_i = \alpha_i \cdot /v/ + \beta_i \qquad (4\text{-}4)$$

Where α_i and β_i are user-specified coefficients.

If Equation (4-4) replaces the K_i in Equation (4-3), the following relationship exists:

$$\partial P = \alpha v^2 + \beta v \qquad (4\text{-}5)$$

where ∂P is the pressure drop in the flow direction and v is the inlet velocity. The coefficients α and β are obtained from the pressure drop versus velocity characteristic obtained from the detailed hydraulic model of a tube row. The coefficients for the tube bank and airheater will be determined in the following sections.

4.4.3 Porosity Characteristics for Boiler Bank Tubes

4.4.3.1 Porosity Characteristics Across Boiler Bank Tubes in Crossflow

The porosity coefficients for the tube bank in crossflow are determined in this section through the use of a CFD hydraulic model. One row of tubes is used to determine the pressure drop versus velocity characteristics of the tube bank. This setup is illustrated in Figure 4-24. The computational domain used in the CFD analysis in this section is the green crosshatched region in Figure 4-24. The figure only shows a few tubes in the flow direction for clarity. In the real model there are 26 rows separated in the middle by a gap.

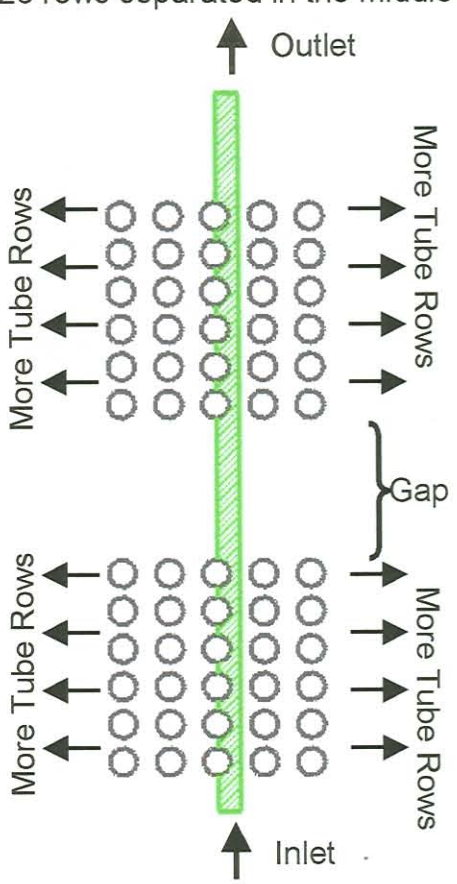

Figure 4-24 Computational Domain to Determine Dressure Drop Characteristcs for Crossflow Configuration

The computational grid around one tube of the domain shown in Figure 4-24 can be seen in Figure 4-25. The whole computational domain consists of 44100 fluid cells. Incompressible air is used as the fluid. The k-ε turbulence model is used and no heat transfer is assumed in the CFD model.

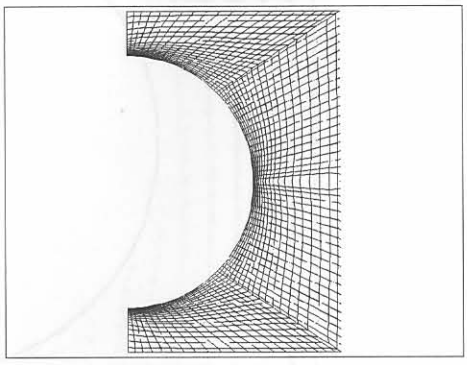

Figure 4-25 Computational Grid for Cross Flow Around One Tube in a Tube Bank (88.9 mm Tube Diameter)

The velocity flow field around only one tube can be seen in Figure 4-26 and Figure 4-27 for an inlet velocity of $7 m.s^{-1}$. Figure 4-26 contains less velocity vectors for clarity but was obtained using the same grid density as in Figure 4-27. The point of separation is clearly visible. No information was found in the literature that gave a correlation for the determination of separation point on a tube for flows in tube banks for the verification of the results. The flow pattern repeats almost identically for subsequent tubes, as can be seen in Figure 4-28. This is consistent with the results of Weaver and Abd-Rabbo[**75**] which stated that turbulence is essentially fully developed by the third row of tubes at high Reynolds numbers. The pressure drop across the whole tube bank for one tube row is illustrated in Figure 4-29. The pressure drops because of the friction drag of the tubes. The pressure is also dropping because of the losses incurred by all the recirculation zones behind the tubes. The pressure drop is a function of fluid flow velocity, number of tube rows, tube spacing in the transverse and longitudinal directions, tube diameter and fluid properties [**85**].

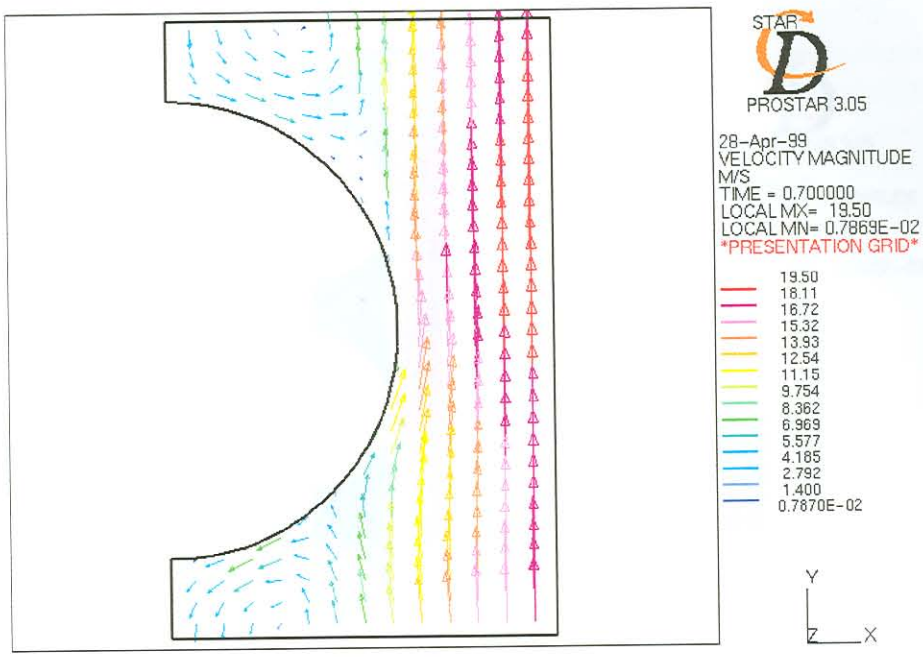

Figure 4-26 Velocity Vectors for Presentation Grid around One Tube of the Boiler Bank for a Crossflow Configuration (7m.s^{-1} Inlet Velocity)

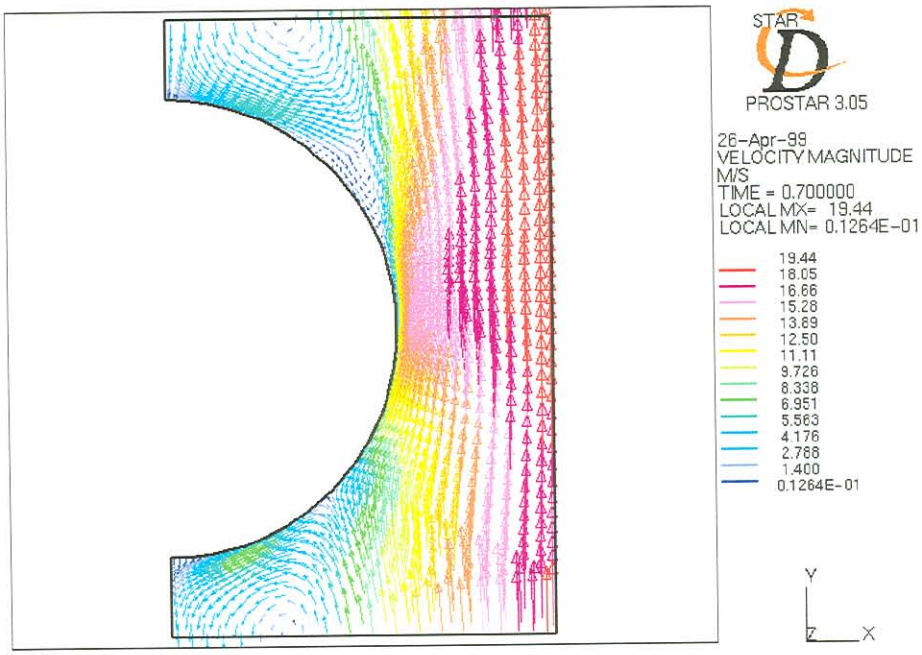

Figure 4-27 Velocity Vectors for actual grid around one tube of the boiler bank for a crossflow configuration (7m.s^{-1} Inlet Velocity)

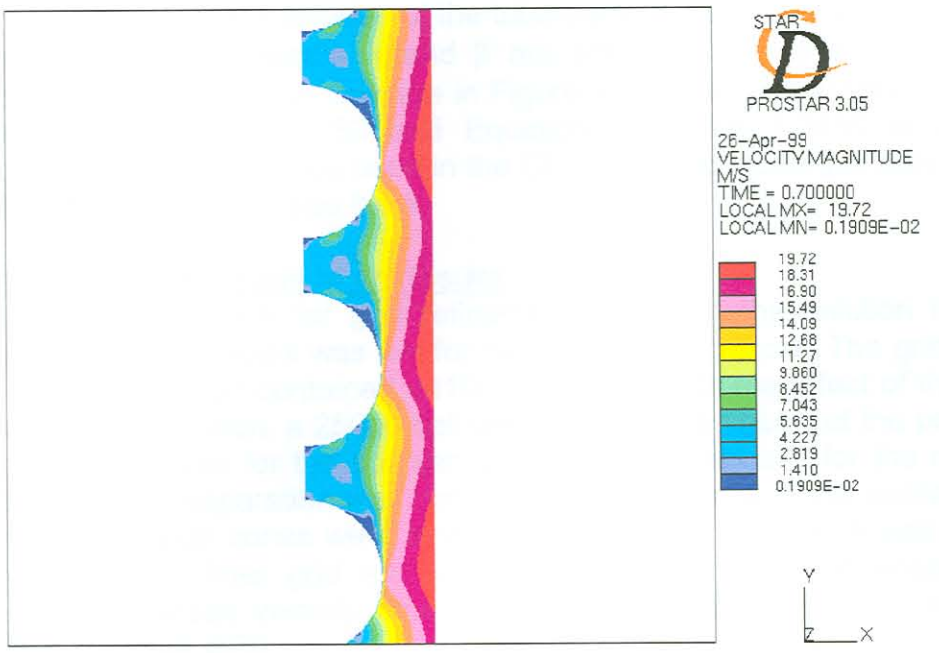

Figure 4-28 Velocity magnitude contour plot for flow around a few tubes of the boiler bank for a crossflow configuration (7m.s^{-1} Inlet Velocity)

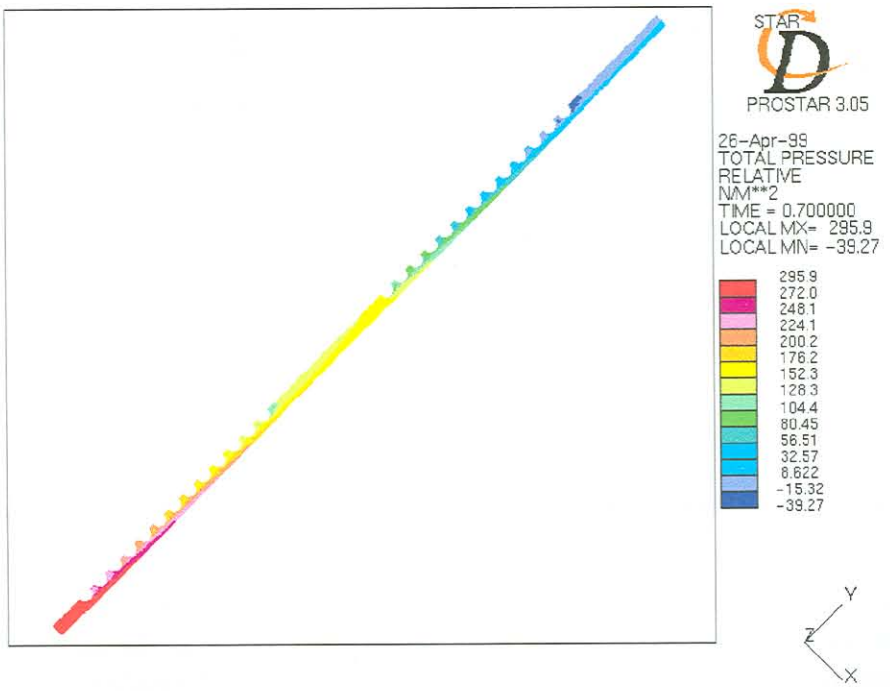

Figure 4-29 Relative pressure distribution over whole computational domain of the boilerbank for a crossflow configuration (7m.s^{-1} Inlet Velocity)

Calculation of the Porosity Coefficients

The pressure drop characteristics of the tube bank in crossflow is illustrated in Figure 4-30. The coefficients α and β are obtained from a second order polynomial curve fit through the data in Figure 4-30. The coefficients α and β from the plot in Figure 4-30 and Equation (4-5) are 1.0436 and 5.84 respectively. This data can be used in the CFD model to model porosity in the crossflow direction of the tube bank.

The Effect of Grid Refinement on Results

It is important to check for grid refinement to see if the solution is grid independent. The analysis was run for two different grid sizes. The grid used in the previous section contained 44100 cells. To check the effect of the grid size on the flow solution, a 25000 cell grid is used. The values of the porosity constants were lower for the coarser grid than was the case for the refined grid. The point of separation was not as clearly defined with the coarse grid and the recirculation zones were smaller. The point of separation was better resolved with the finer grid and thus better results were obtained. The pressure drop versus velocity characteristics for the two different cases is illustrated in Figure 4-30.

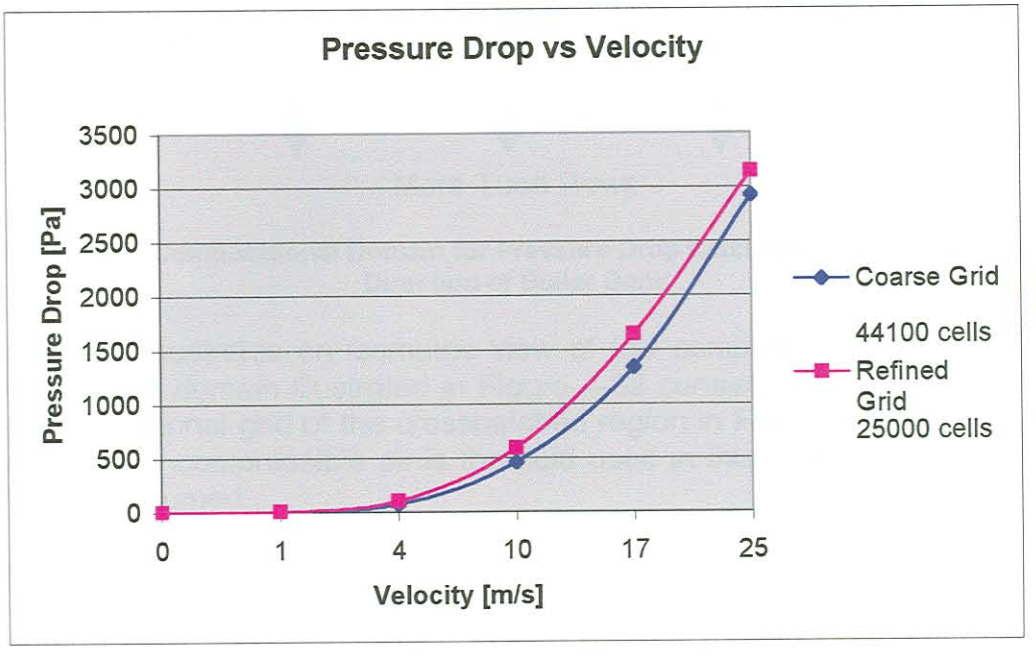

Figure 4-30 Pressure drop versus velocity characteristic for the whole tube bank for a crossflow configuration.

Because of some difficulties with stability in the CFD model with boiler internals, which will be discussed later, it was decided to determine the porosity coefficients in the longitudinal directions of the tubes as well. Although the pressure drop will be much less in this direction compared to the cross flow direction, it is important to obtain this resistance to the flow. This will simulate the porosity characteristics of the tube bank much more accurately.

4.4.3.2 Porosity Characteristics of Flow in the Longitudinal Direction of Tubes

The domain for the calculation of pressure drop in the longitudinal direction of a tube bank is illustrated as the green crosshatched region in Figure 4-31. Symmetry boundary conditions are used in all four directions shown in Figure 4-31. The flow direction in Figure 4-31 is into the page.

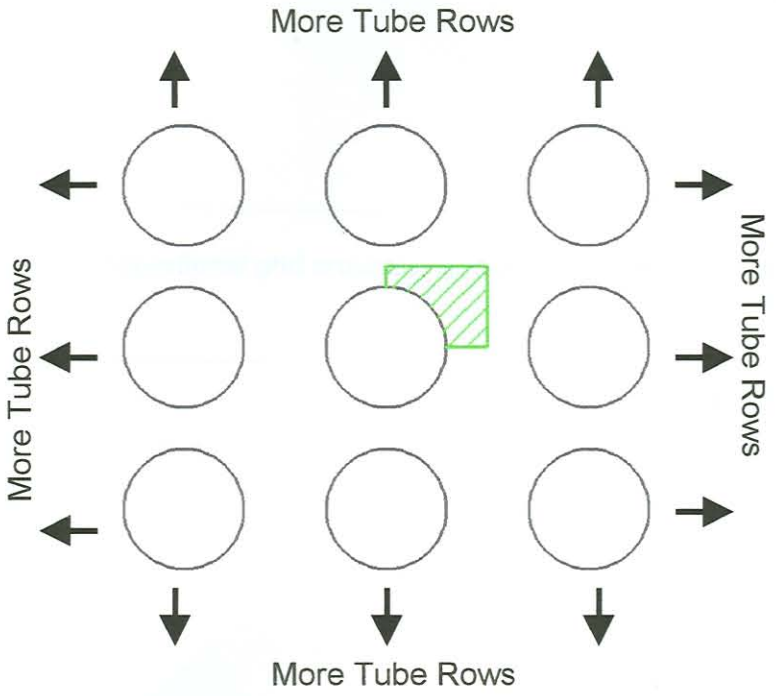

Figure 4-31 Computational Domain for Pressure Drop Calculation in Longitudinal Direction of Boiler Bank

Figure 4-32 illustrates an isometric view of the computational domain. The computational domain illustrated in Figure 4-32 consists of 25500 fluid cells. The computational grid of the crosshatched region in Figure 4-31 is shown in Figure 4-33. Incompressible air is the fluid used in this analysis and no heat transfer is assumed.

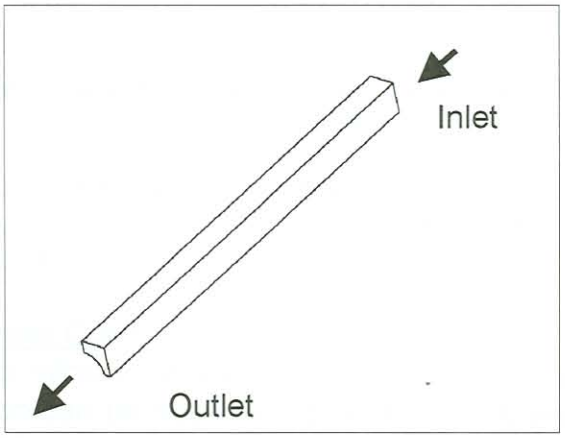

Figure 4-32 Edge plot of computational domain for flow parallel to the boiler bank tubes

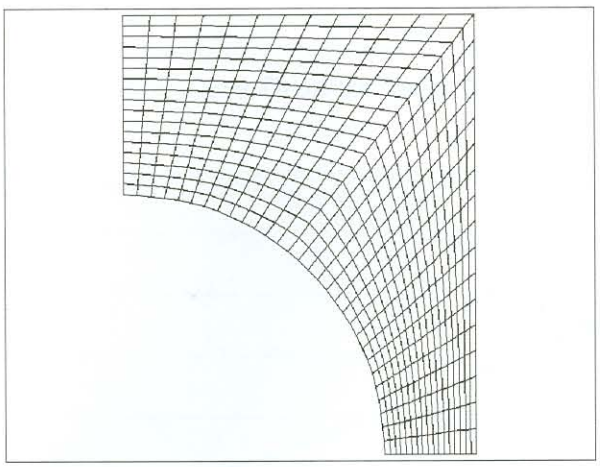

Figure 4-33 Computational grid around one tube for flow parallel with the tube

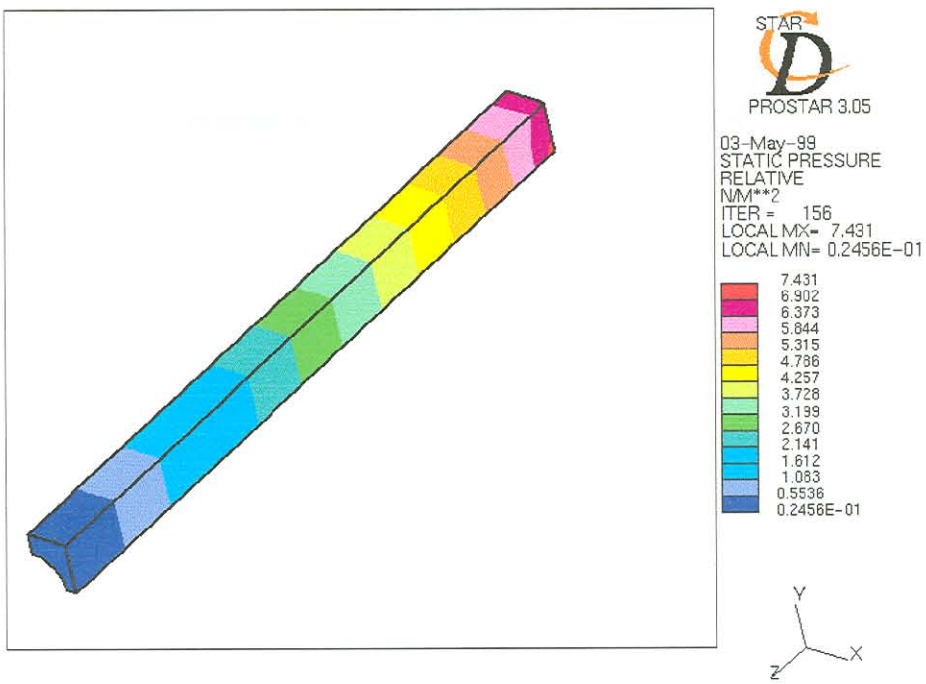

Figure 4-34 Pressure drop in the longitudinal direction around one boiler bank tube ($10m.s^{-1}$ Inlet Velocity)

The pressure drop across the computational domain for a unit length of tube is illustrated in Figure 4-34 for an inlet velocity of $10m.s^{-1}$. The pressure drops because of tube wall friction.

Calculation of Porosity Coefficients

The pressure drop versus velocity characteristic of the tube bank in the longitudinal direction can be seen in Figure 4-35. The porosity coefficients α and β are obtained from a second order polynomial curve fit through the data in Figure 4-35. From the data in Figure 4-35 and Equation (4-5), the two porosity coefficients, α and β, are 0.0194 and 0.5016, respectively.

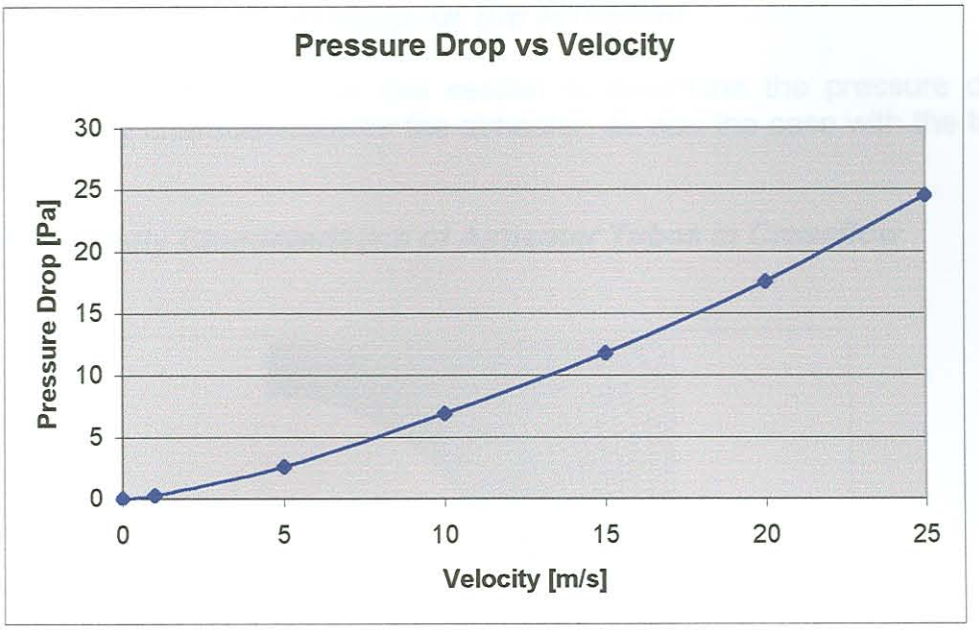

Figure 4-35 Pressure drop versus Velocity characteristic for boiler bank tubes in the longitudinal direction

4.4.4 Porosity Characteristics for the Airheater

The same method is used in this section to determine the pressure drop versus velocity characteristics for the airheater, as was the case with the tube bank.

4.4.4.1 Porosity Characteristics of Airheater Tubes in Crossflow

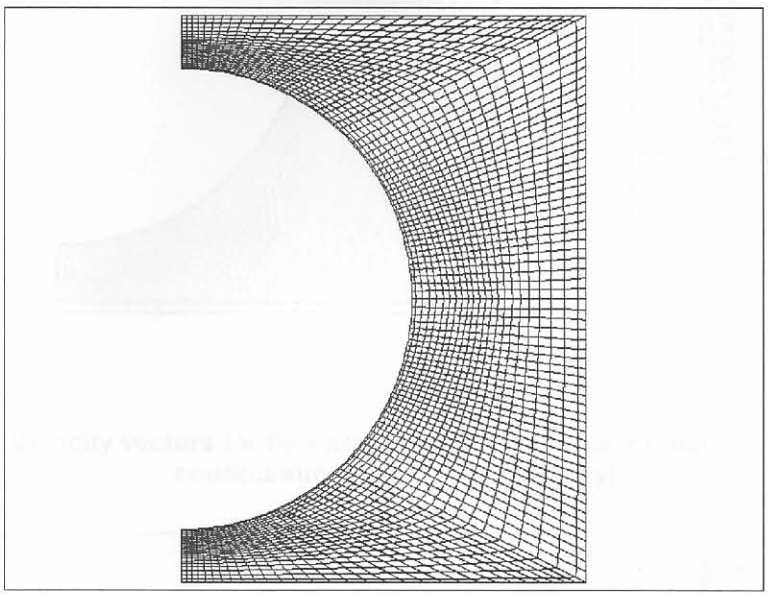

Figure 4-36 Computational grid for the airheater around one tube for a crossflow configuration. (57mm Tube Diameter)

The computational domain for this CFD analysis consisted of 28000 fluid cells. The computational grid around one tube can be seen in Figure 4-36. The velocity vector field around one tube is illustrated in Figure 4-37 for an inlet velocity of $7m.s^{-1}$. The recirculation zones in front and at the back of the tube is clearly seen. The recirculation zones and tube wall friction are the main factors contributing to pressure contour plot across the computational domain. The pressure drop across some of the airheater tubes is illustrated in Figure 4-38.

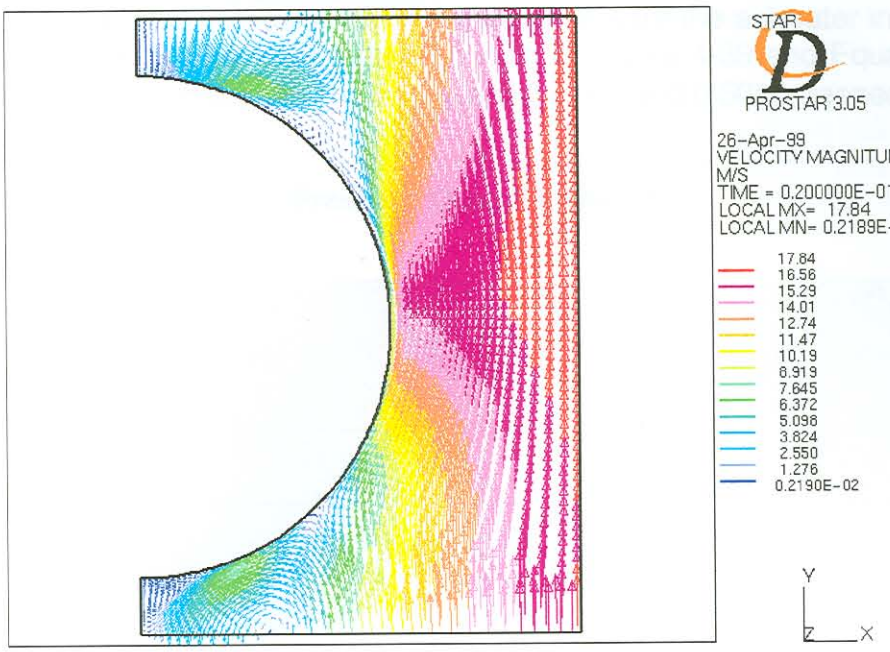

Figure 4-37 Velocity vectors for flow around one tube of the airheater for a crossflow configuration (7m.s^{-1} Inlet Velocity)

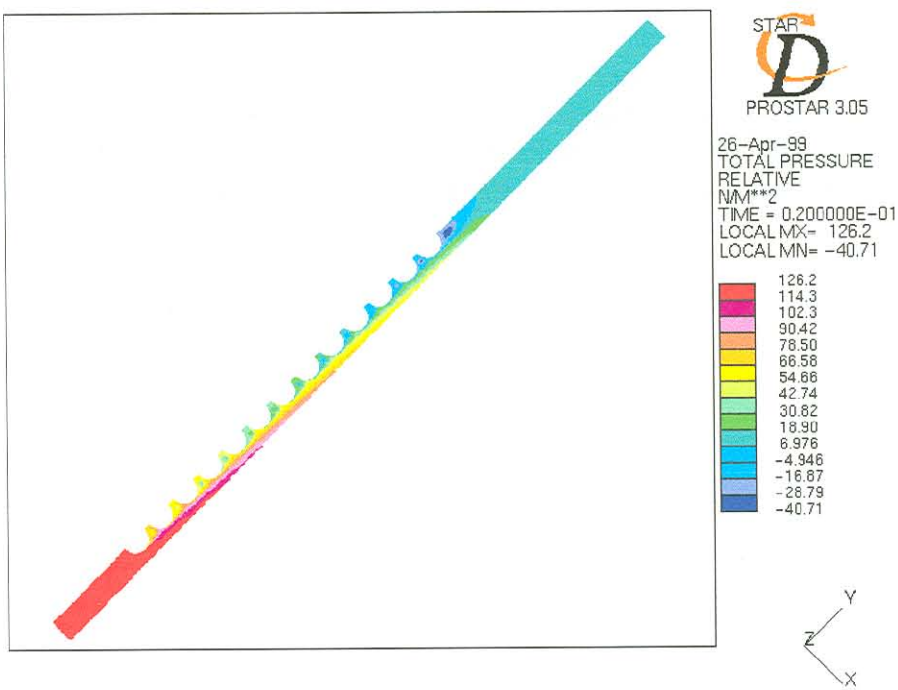

Figure 4-38 Pressure drop across tubes of the airheater for a crossflow configuration (7m.s^{-1} Inlet Velocity)

Calculation of Porosity Coefficients

The pressure drop versus velocity characteristics for the airheater in crossflow is illustrated in Figure 4-39. From the data in Figure 4-39 and Equation (4-5) the two porosity coefficients, α and β, are 0.0194 and 0.5016, respectively.

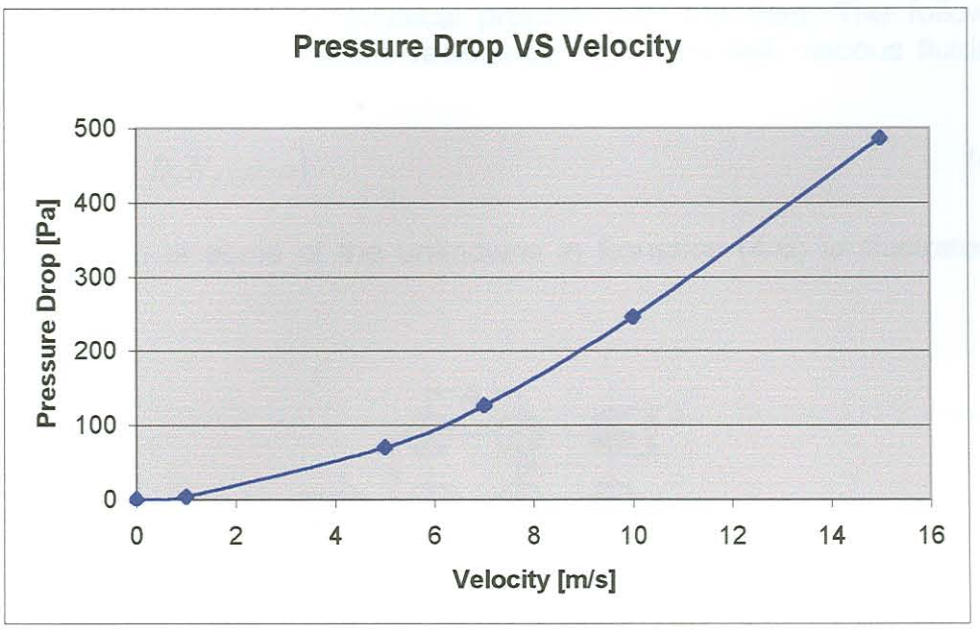

Figure 4-39 Pressure Drop versus Velocity characteristic for the air heater for a crossflow configuration

Because of stability problems in the CFD model of the overall CFD boiler model, the pressure drop versus velocity characteristics was not determined for the airheater tubes in the longitudinal direction. This also proved unnecessary because it was decided not to include the effect of the airheater in the overall boiler CFD model.

4.4.5 Comparison of Numerical Results to Empirical Data

Zukauskas[**85**] studied the hydraulic resistance of tube banks. He said that the total pressure drop across a bank of tubes is a function flow velocity, tube bank arrangement and the physical properties of the fluid. The following functional relation expresses the resistance of a bank with viscous fluids of constant density:

$$\Delta p = f\left(V, S_T, S_L, D, N_L, \mu, \rho\right) \tag{4-6}$$

The description of some of the unknowns in Equation (4-6) is illustrated in Figure 4-40.

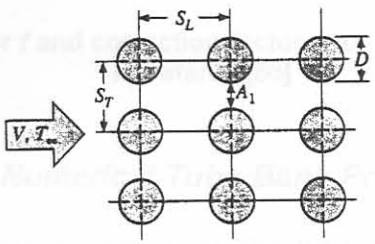

Figure 4-40 Tube Arrangement Parameters [94]

The dimensionless form of the relation discussed above are:

$$Eu = \phi\left(\mathrm{Re}, \frac{S_T}{D}, \frac{S_L}{D}, N_L\right) \tag{4-7}$$

The pressure drop across a bank of tubes can be expressed as:

$$\Delta p = N_L \chi \left(\frac{\rho V_{\max}^2}{2}\right) f \tag{4-8}$$

The values of f and χ are obtained from the Moody-type graph in Figure 4-41 and the value of V_{max} is obtained from Equation (4-9):

$$V_{maks} = \frac{S_T}{S_T - D} V \tag{4-9}$$

V_{max} is used because the correlations are based on maximum fluid velocity within the tube bank. For an in-line tube bank, V_{max} occurs at the transverse plane A_1 of Figure 4-40.

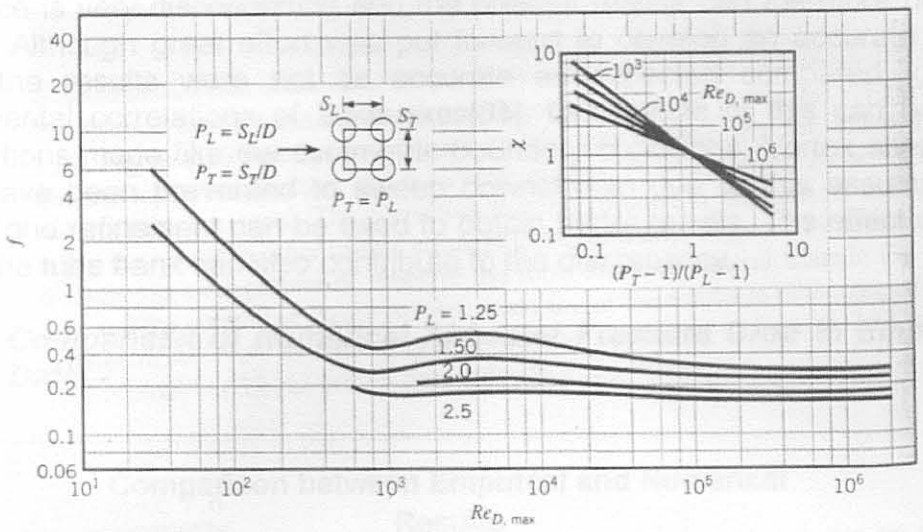

Figure 4-41 Friction factor *f* and correction factor χ for the calculation of hydraulic resistance[86]

4.4.5.1 Comparison of Numerical Tube Bank Pressure Drop to Empirical Pressure Drop

The calculation of pressure drop through the tube bank using the correlations developed by Zukauskas[**85**] can be seen in Appendix B. A MS Excel macro was used to determine the pressure drop. The same solution strategy was followed as was used by Incropera and DeWitt[**94**].

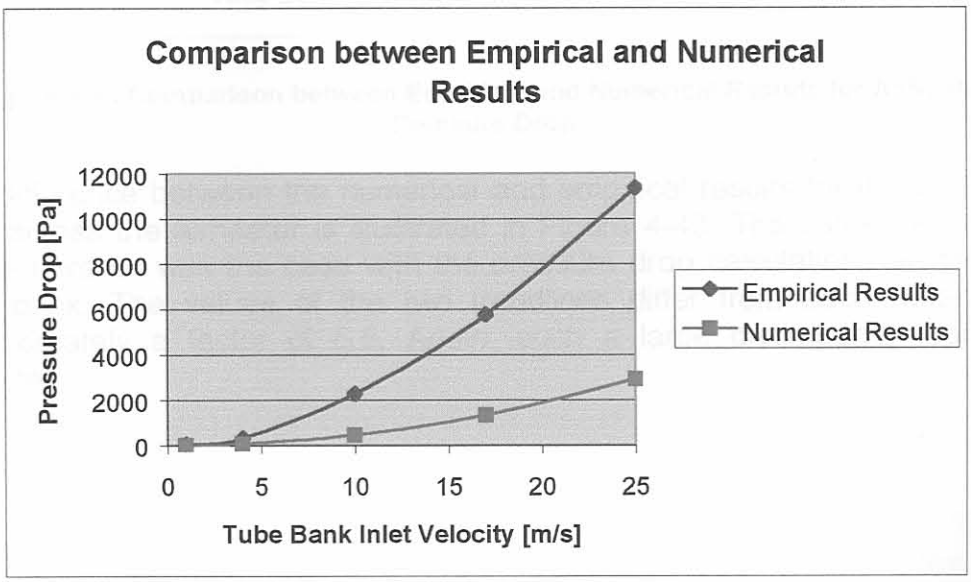

Figure 4-42 Comparison between Empirical and Numerical Results for Tube Bank Pressure Drop

The numerical results obtained in Chapter 4.4.3.1 for the tube bank and the results from the experimental correlations of Zukauskas[**85**] are plotted in Figure 4-42. The empirical correlation predicts a pressure drop with a factor of 4 higher than the numerical results obtained in this study. This large

difference is very disconcerting and the present results can therefore not be trusted. Although great effort was put forward to develop an accurate CFD model the results were not as accurate as expected compared to the experimental correlations of Zukauskas[**85**]. One cause of this can be the assumptions made like the symmetric boundary conditions. Vortex shedding could have been prevented to sweep downstream due to this assumption. Further grid refinement can be used to obtain better results. The effect of the gap in the tube bank can also contribute to the discrepancy.

4.4.5.2 Comparison of Numerical Airheater Pressure Drop to Empirical Data

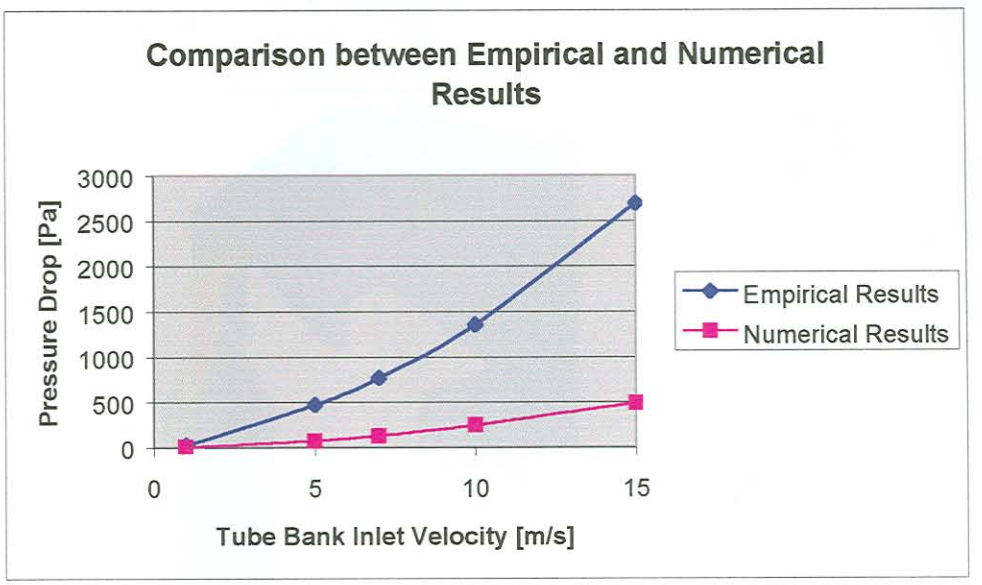

Figure 4-43 Comparison between Empirical and Numerical Results for Airheater Pressure Drop

The difference between the numerical and empirical results for the pressure drop across the airheater is illustrated in Figure 4-43. The same trends are visible here as was the case with the pressure drop calculations across the tube bank. The values of the two trendlines differ from each other with approximately a factor of 5.5. Again, such a large discrepancy was not expected.

4.4.6 Application of Porosity Coefficients to Boiler Internals

Although the porosity coefficients determined for the boiler internals are not trustworthy, porous sections will still be used in the CFD boiler models to see what effect they have on the flow pattern through the boiler.

4.4.6.1 Application of Porosity Coefficients to the Boiler Bank

To simulate the effect of the boiler bank, porous cells were placed in the location of the boiler bank. The characteristics of the porous cells were determined in Chapter 4.4.2. The same approach was followed by Vakkilainen et al.[**90**] with the use of porous cells to replace the boiler bank in the CFD model of the boiler.

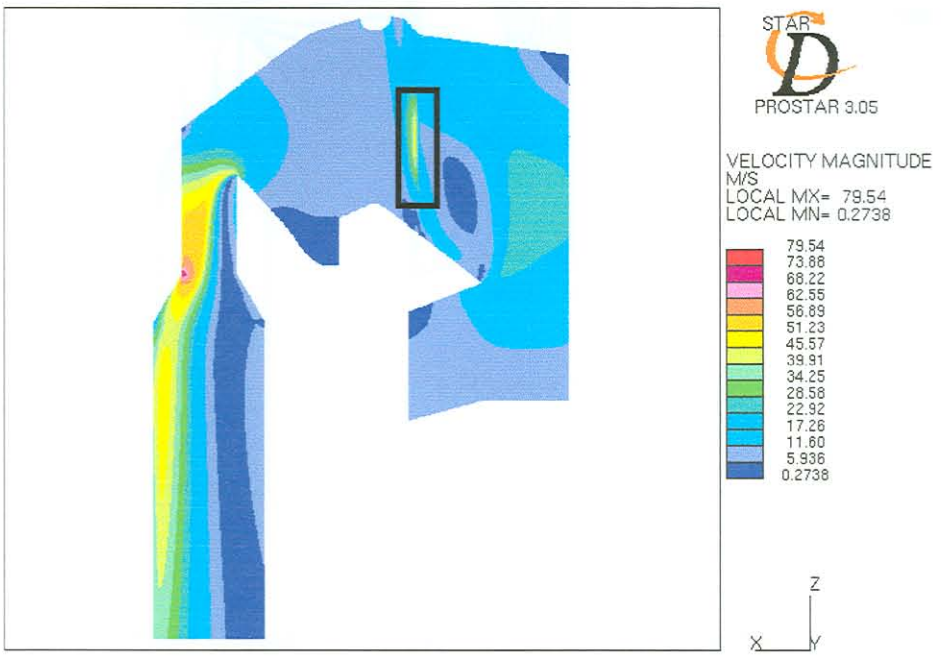

Figure 4-44 Velocity Magnitude Plot for Boiler Model with Porous Cells to Replace Tube Bank (10m.s^{-1} Inlet Velocity)

The velocity magnitude plot for the boiler model with boiler bank modelled as porous cells, is illustrated in Figure 4-44. As can be seen in the rectangle in Figure 4-44 for an inlet velocity of 10m.s^{-1}, the flow field at the entrance of the boiler bank is not realistically represented. Because the resistance of flow in the vertical direction of the tube bank is less than in the cross-flow direction, the flow is turned vertically downwards to follow the path of least resistance. This is due to the directional properties of the porous cells used to 'replace' the boiler bank. Except for the flow that is indicated in the rectangle in Figure 4-44, the rest of the flow field seems to be realistic. Vakkilainen et al.[**90**] found that the modelling of flow without boiler internals gave better results for flow patterns through boiler than models with internals. The results of this study are thus in agreement with other researchers' work.

Figure 4-45 and Figure 4-46 illustrate the particle trajectories for 10μm and 100μm particles respectively. The result in Figure 4-45 does not resemble erosion patterns that were observed during boiler shutdown. The porous section in the CFD model redistributes the ash particles across the whole crossflow area of the tube bank. Better results were obtained where no boiler internals were modelled. Refer to Figure 4-12 for the illustration of particle trajectories where no boiler internals were used. The particle trajectories for 100μm particles illustrated in Figure 4-46 are more consistent with observed erosion patterns during boiler shutdown.

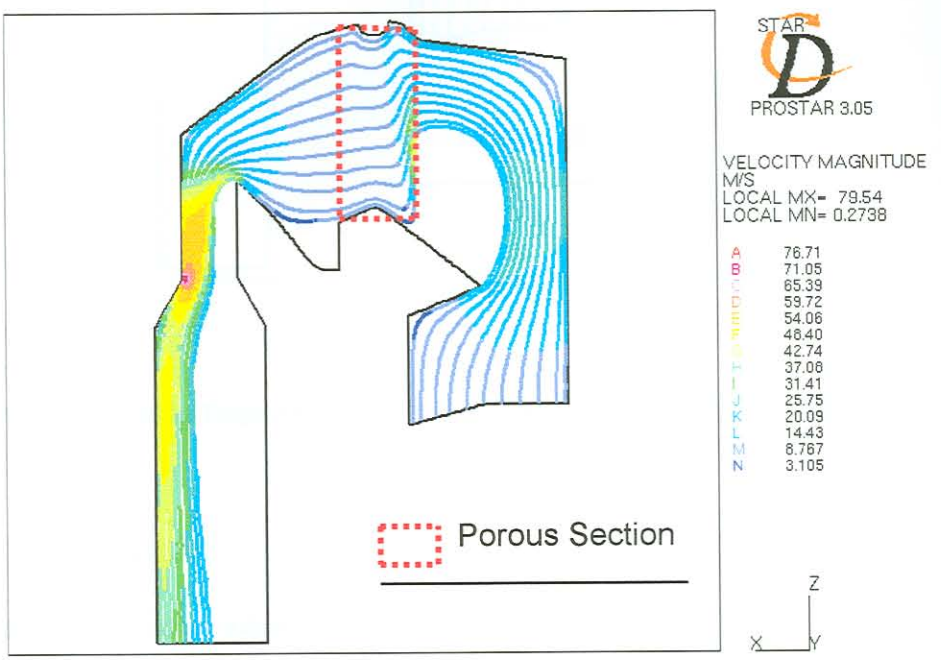

Figure 4-45 Particle Trajectories for 10μm Particles with Porosity Model included for the Boiler Bank

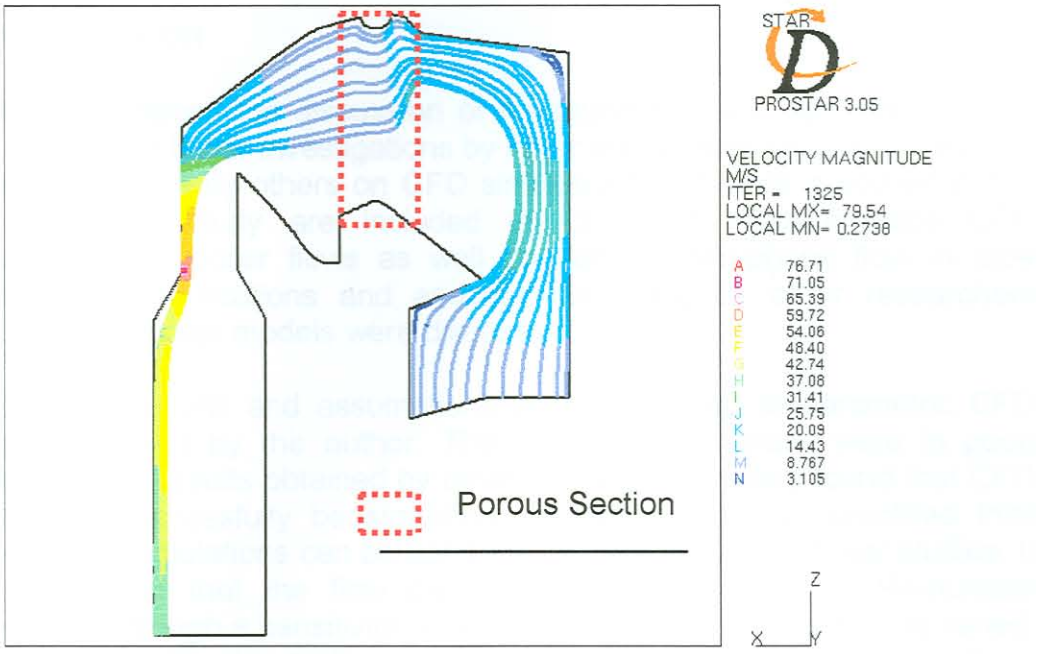

Figure 4-46 Particle Trajectories for 100μm Particles with Porosity Model included for the Boiler Bank

4.4.7 Conclusion

In this section ways were investigated to simplify boiler internals in boiler CFD models. The proposed method was to determine the pressure drop versus velocity characteristics in a detailed hydraulic model of one row of the boiler bank. The pressure drop versus velocity characteristics were then used to define porous cells in the CFD model with the same pressure drop characteristics. The results obtained numerically differ from the experimental correlations of Zukauskas[**85**]. No concrete explanation can be given for the large difference in the computational and experimental results. When the porous cells were included in the 2D CFD model, the results were reasonable with the exception of the flow field at the inlet of the tube bank. It can be concluded, however, that the usage of porous cells to replace boiler internals gives rise to too many uncertainties to use them in detailed CFD boiler models. Due to time constraints to complete this thesis it was decided to not use porous sections for the further CFD analyses in this study. For future work following this study, it is recommended that the uncertainties arising from this study be investigated in more detail to obtain reliable methods to replace boiler internals. The advice of Tu et al. [**48**] is followed in this study that it is possible to obtain a good indication of regions of high erosion rate without the need of modelling tube banks. Tu et al. [**48**] stated that the quality of solutions in boilers without tube banks is sufficient to provide an insight into the flow phenomena and erosion patterns within coal-fired boilers.

4.5 Conclusion

Chapter 3 contained the discussion of the found that was applicable to this study, except for boiler investigations by other researchers regarding CFD. All the research done by others on CFD simulations that were important in the context of this study are included in Chapter 4. This includes CFD investigations on boiler flows as well as detailed two-phase flow in tube banks. The simplifications and assumptions made by other researchers regarding CFD boiler models were discussed.

These simplifications and assumptions were compared to parametric CFD studies performed by the author. The results of this study were in good agreement with results obtained by other researchers. It was found that CFD models can successfully be simplified through the use of simplified inlet geometry. 2D simulations can be used with success in centre boiler studies. It was also found that the flow pattern through the boiler is Re-number independent through a sensitivity analysis where the inlet velocity was varied. It was also found in this CFD parametric study that larger particles are flung towards the top of the boiler to a larger extent than smaller particles due to higher inertial forces.

In the section that concluded this chapter, boiler internals were simplified through the use of porous sections. The pressure drop versus velocity characteristic of the boiler internals were obtained through a detailed hydraulic model. These results did not compare well to experimental data published by another researcher and more work is necessary to obtain more reliable results. This can include the comparison of the results to other experimental correlations.